2018

An Energy Harvesting Solution for IoT Sensors Using MEMS Technology

Maryam Eshaghi
University of Windsor

An Energy Harvesting Solution for IoT Sensors Using MEMS Technology

By

Maryam Eshaghi

A Thesis

Submitted to the Faculty of Graduate Studies

through the Department of Electrical and Computer Engineering

in Partial Fulfillment of the Requirements for

the Degree of Master of Applied Science

at the University of Windsor

Windsor, Ontario, Canada

2018

An Energy Harvesting Solution for IoT Sensors Using MEMS Technology

by

Maryam Eshaghi

APPROVED BY:

_____

A. Azab

Mechanical, Automotive & Materials Engineering

_____

S. Erfani

Department of Electrical and Computer Engineering

_____

R. Muscedere, Co-Advisor

Department of Electrical and Computer Engineering

_____

R. Rashidzadeh, Co-Advisor

Department of Electrical and Computer Engineering

June 14, 2018

DECLARATION OF ORIGINALITY

I hereby certify that I am the sole author of this thesis and that no part of this thesis has been published or submitted for publication.

I certify that, to the best of my knowledge, my thesis does not infringe upon anyone's copyright nor violate any proprietary rights and that any ideas, techniques, quotations, or any other material from the work of other people included in my thesis, published or otherwise, are fully acknowledged in accordance with the standard referencing practices. Furthermore, to the extent that I have included copyright material that surpasses the bound of fair dealing within the meaning of the Canada Copyright Act, I certify that I have obtained a written permission from the copyright owners(s) to include such material(s) in my thesis and have included copies of such copyright clearances to my appendix.

I declare that this is a true copy of my thesis, including any final revisions, as approved by my thesis committee and the Graduate Studies office, and that this thesis has not been submitted for a higher degree to any other University or Institution.

ABSTRACT

The significant development of IoT sensors will play a critical role in a large number of applications. It is predicted that billions of IoT sensors will be used worldwide by 2020 [1]. Batteries are commonly utilized to power on sensors, but they are depleted and they require maintenance and replacement. Battery replacement for billions of sensors is a daunting task and battery disposal for IoT sensors can become an environmental problem. Energy harvesting from ambient sources presents a viable solution to overcome these problems. Among all energy sources, light is considered as one of the best sources due to its high energy density and availability in both indoor and outdoor environments. In order to make an energy harvesting system efficient, many methods have been proposed in the literature to extract the maximum energy while minimizing the power consumption by the energy harvesting circuitry.

In this work, a boost converter circuit is designed using MEMS-based switches to reduce the leakage current and power loss caused by conventional transistor-based switches. A light energy harvesting method is also proposed utilizing available components of a typical IoT sensor. The reuse of available components in the proposed solution reduces the overall power consumption and the area overhead of the energy harvesting solution.

DEDICATION

I dedicated this thesis to my Mother and Father who spent their life on educating science to students. They always have encouraged me to continue my education. They taught me how to start with A, B, C and finish with a Master of Science dissertation. I am very thankful for their support, patience, and encouragement.

A world of thanks goes to my love and my husband, Mehran Aliasgarian. I am really grateful for his enthusiasm, support, collaboration, and encouragements during my research.

ACKNOWLEDGMENTS

I would like to sincerely thank my supervisor, Dr. Rashid Rashidzadeh, for his guidance and support to complete my thesis. I am deeply grateful for his time, weekly meetings and technical comments during my research and study. It is an honor to work under his supervision.

I am grateful to my co-supervisor Dr. Roberto Muscedere for his support and valuable comments which helped in completing this thesis.

I would also like to thank my committee members Dr. Shervin Erfani and Dr. Ahmed Azab for their, encouragement, constructive comments and positive criticism which in fact improved my ideas and solutions.

I would like to extend my gratitude to my colleagues at the Research Centre for Integrated Microsystems (RCIM). I appreciate their friendship, support, encouragement, their constant involvement and valuable feedback.

Finally, I would like to thank the research and financial support received from Natural Sciences and Engineering Research Council (NSERC) of Canada and CMC Microsystems.

TABLE OF CONTENTS

LIST OF TABLES

LIST OF FIGURES

LIST OF ACRONYMS

Abbreviations	Description
ADC	Analog to Digital Converter
CCM	Continues Current Mode
DC-DC	Direct Current to Direct Current
DCM	Discontinues Current Mode
FET	Field Effect Transistor
FOM	Figure Of Merit
IoT	Internet of Things
MCU	MicroController Unit
MEMS	Micro Electro Mechanical Systems
MOSFET	Metal-Oxide-Semiconductor Field-Effect Transistor
MPP	Maximum Power Point
OC	Open Circuit
PCB	Printed Circuit Board
PIN	P-I-N (diode switch)
PV	Photovoltaic
PWM	Pulse Width Modulation
RF	Radio Frequency
SC	Short Circuit
TEM	Thermo Electro-Mechanical

CHAPTER I

INTRODUCTION

1.1 Internet of Things (IoT)

A network of physical devices combined with electronic sensors and connected to the Internet is called Internet of Things (IoT) as shown in Figure 1.1. These devices can collect data from surrounding environment, communicate with each other, and exchange the information [2]. Connected objects can provide valuable information from their nearby environment [3].

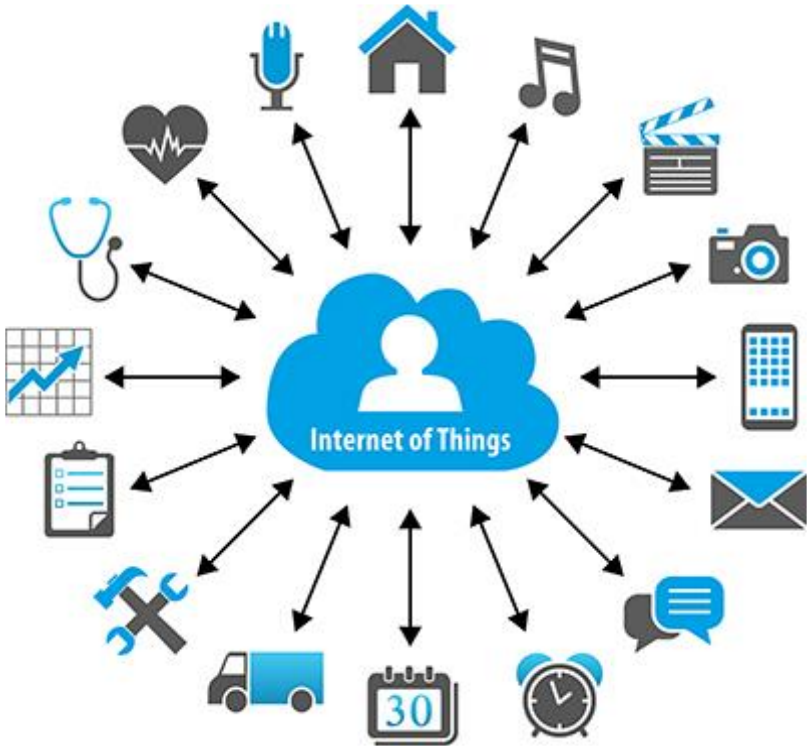

Figure 1.1 Internet of Things [4]

Figure 1.2 An example picture of IoT sensors [5]

Wireless sensor nodes or IoT devices are placed in different places to monitor various parameters and collect data from nearby sources and exchange the data with other devices for different purposes [6]. A wireless sensor node can be used for different applications including environmental monitoring, medical care, military surveillance, automotive manufacturing, supply chain tracking, etc [7]. Figure 1.2 represents an example of IoT sensor.

1.2 IoT Sensor Challenges

Sensors which are needed to be plugged have limited applications as they cannot be far from a power outlet. Today, wireless sensors are usually powered on with batteries which make them attractive for many applications. However, batteries get depleted after a while and they have to be replaced. This can be a serious problem if the number of deployed IoT sensors is taken into consideration. Battery maintenance and replacement for billions

Figure 1.3 Various source of energy in environment [10]

of wireless sensors can be very costly and time-consuming [8]. Another important problem is the battery disposal and pollution due to dangerous toxic chemical material in batteries which can contaminate the environment and cause animal and human diseases [9]. Energy harvesting solutions from environment sources emerge as viable solutions to power up IoT sensors.

1.3 Energy Harvesting and Ambient Sources

IoT devices are designed to consume the minimum amount of power and the enough energy required to turn them on can commonly be extracted from the ambient sources using energy harvesting techniques.

There are many ambient sources as shown in Figure 1.3 that can be the used for energy harvesting. Among them, some sources are suitable for energy harvesting for IoT applications in indoor places including light, thermal, vibration, radio frequency, etc. The

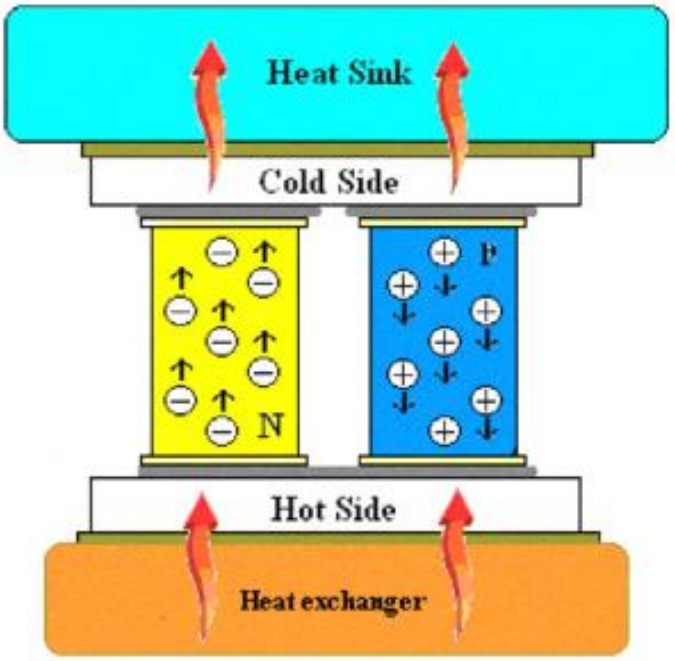

Figure 1.4 The heat flow creates energy which can be harvested to generate electricity [11]

availability and the energy density of these sources determine which source can be utilized for a specific application.

1.3.1 Thermal Energy Harvesting

Thermoelectric generators are utilized to convert thermal energy to electricity using the heat flow between two objects or environments with different temperatures. As shown in Figure 1.4, a thermoelectric generator can be placed in the area between the low and the high temperature and utilize the heat flow for energy harvesting through a thermoelectric generator [12].

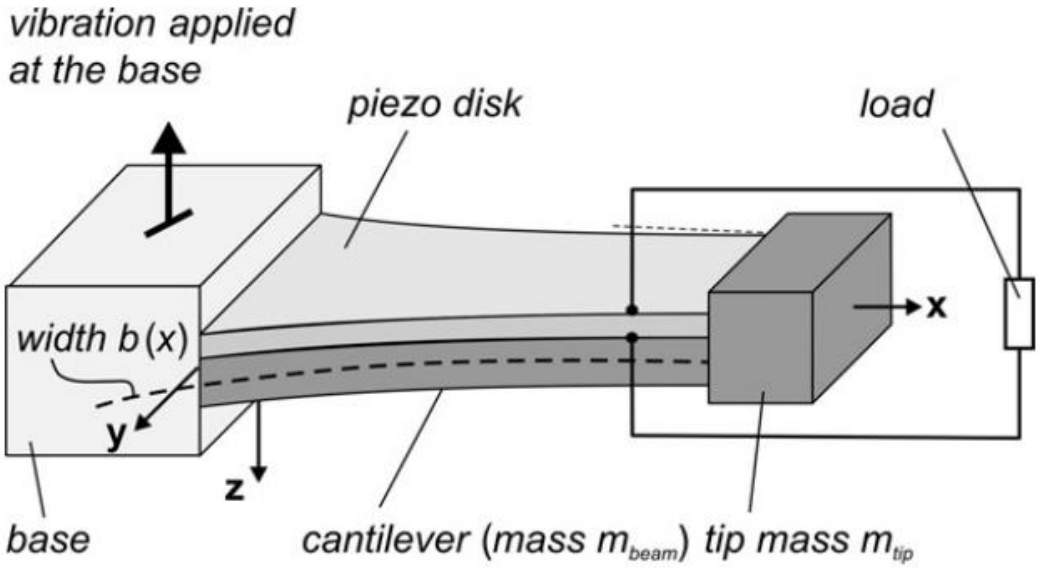

Figure 1.5 General piezoelectric vibration which generates electricity [13]

1.3.2 Vibrational Energy Harvesting

Motion can create vibrational energy and a power generator can convert the kinetic energy into electrical energy. The vibrational energy can be harvested using piezoelectric devices. When piezoelectric materials are exposed to vibration, they accumulate charges and convert the kinetic energy (vibration) to electrical energy [12]. A conventional piezoelectric cantilever beam is shown in Figure 1.5.

1.3.3 Radio Frequency (RF) Energy Harvesting

Radio waves are everywhere due to the radiation by radio and TV transmitters, cellphone towers, WiFi access ports and etc. Researchers have conducted studies to harvest energy from electromagnetic waves [12]. Passive RFID tags receive their energy from the waves transmitted by RFID readers. The building blocks of an RF energy harvester include an efficient antenna to receive the electromagnetic waves, an AC to DC converter to rectify

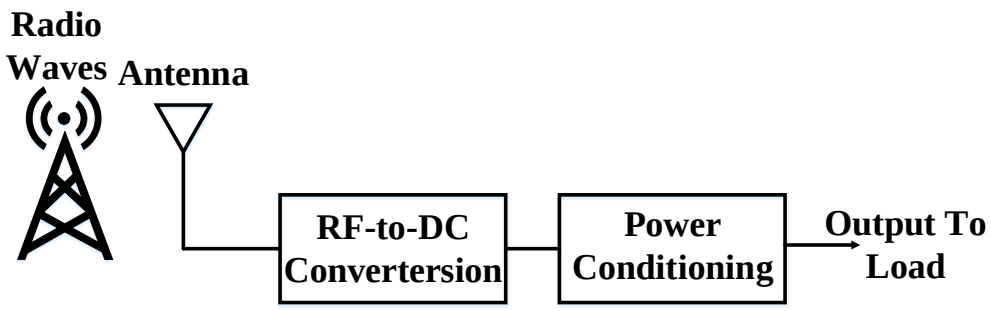

Figure 1.6 Conventional RF energy harvesting system

the induced alternating current to direct current to generate electric energy [15]. Figure 1.6 presents a typical RF energy harvesting system [14].

1.4 Light Energy Harvesting

Among the available energy sources for harvesting, light is the most abundant source in both indoor and outdoor locations. Light has also the highest energy density by the volume unit for low-power systems. Most of the indoor environments including buildings and rooms have enough light energy to power the IoT sensors. The amount of the light energy in indoor environments is commonly much lower than outdoor environments [8]. Nevertheless, the level of light intensity in a typical indoor location is enough to power on the available IoT sensors in the current market. IoT sensors that consume even less power are expected to be designed as the low power design techniques evolve. Figure 1.7 represents a typical energy harvesting system which consists of an energy extractor device, a power converter circuit which can be either a DC-DC converter or AC-DC converter, and a storage element. As shown in Figure 1.8, a conventional light energy harvesting system includes three parts, (a) PV cell, (b) converter and (c) storage element.

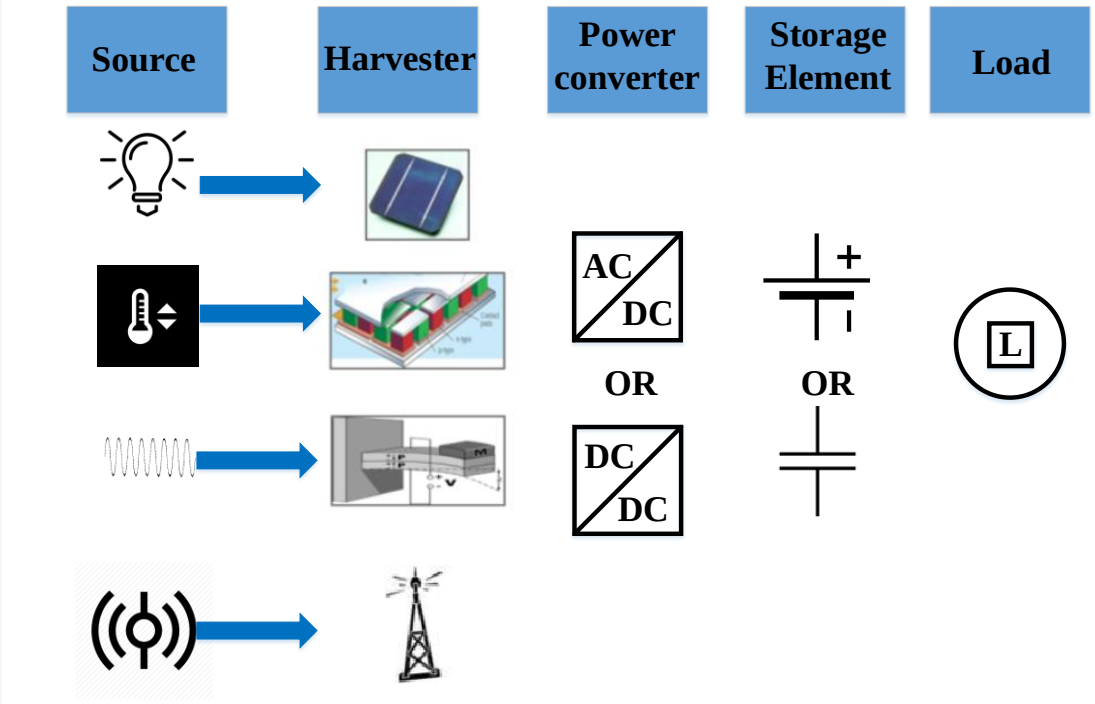

Figure 1.7 A typical energy harvesting system

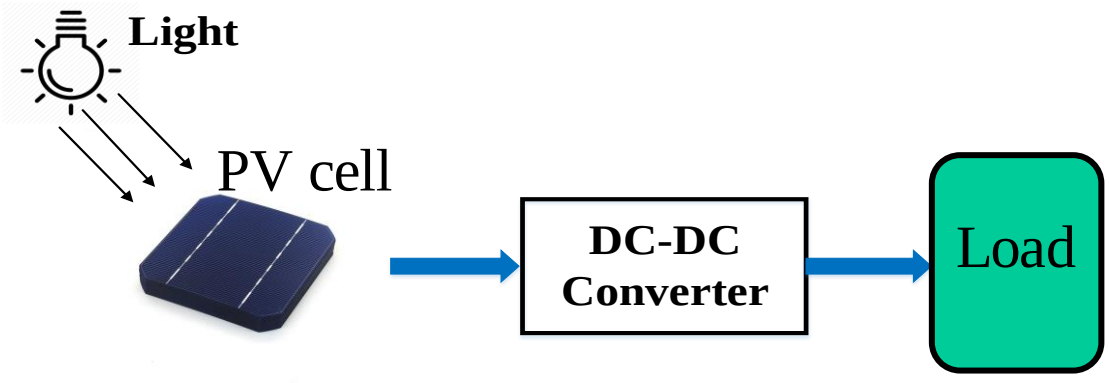

Figure 1.8 Three main parts which are utilized in a conventional light energy harvesting

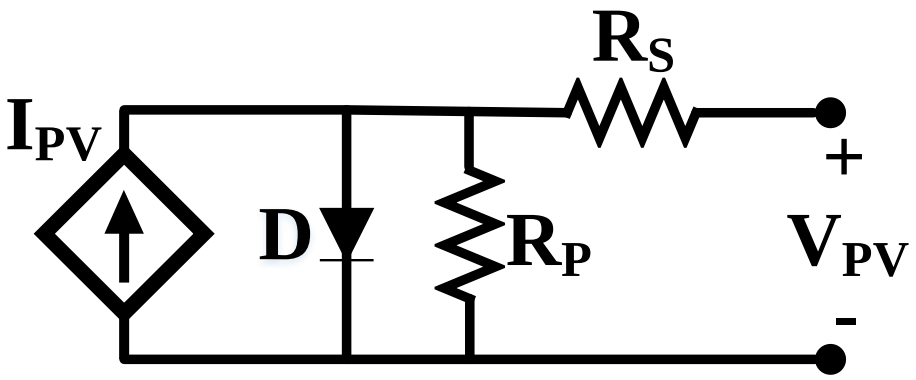

Figure 1.9 The equivalent circuit of a PV cell

A PV cell is an important part of light energy harvesting system which is a specialized semiconductor device or a photodiode that converts light energy to direct current. A PV cell can be modeled by a current source which is in parallel with a diode and a resistor, Rp, [16] as shown in Figure 1.9. The non-ideality of the PV cell is modeled by a shunt resistance, R_P, and a series resistance, R_S. A PV cell has an optimal point of operation where the maximum energy is harvested. The plot of current versus voltage of a PV cell is shown in Figure 1.10. To fully utilize the ambient light energy and to deliver the maximum power to the load, a DC-DC converter is used to supply the load with its nominal voltage. A storage element that can be either a rechargeable battery or a super capacitor is used to store the energy and support continuous operation of the system.

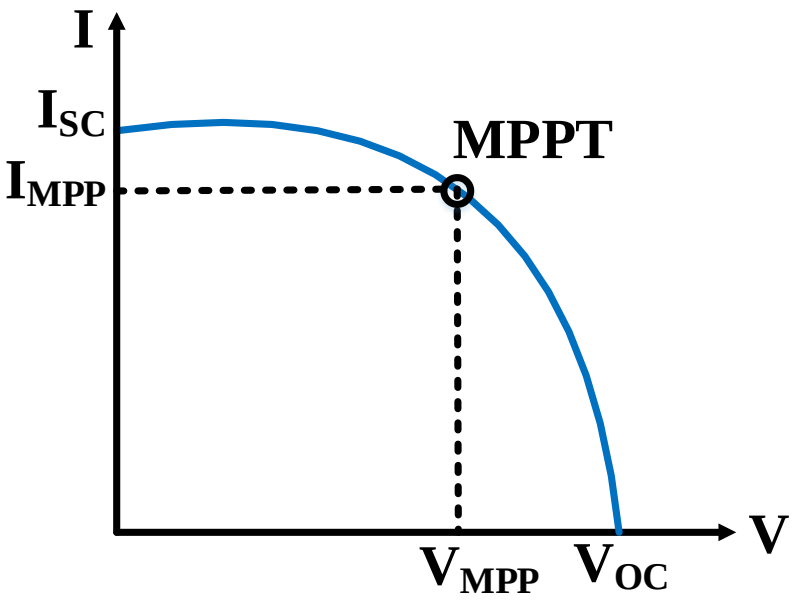

Figure 1.10 Voltage and current characteristics of a typical PV cell

1.4.1 DC-DC Converter

A DC-DC converter is a power converter which converts a source of current with a certain voltage level to a higher or a lower voltage level [17]. As the system must effectively deliver the stored energy and harvested energy to the load, a smart power management strategy is a must for energy harvesters. It is necessary for a harvesting system to design an efficient DC-DC converter between the PV modules and the storage elements to extract the maximum energy from the available source and deliver it to the load or the storage element with a high efficiency and minimum loss as shown in Figure 1.11 [18]. The design of DC-DC converter depends on the operating voltage range of storage element and supply voltage level required by the load. A buck-boost converter is required when the supply voltage is within the voltage range of the storage element since the storage

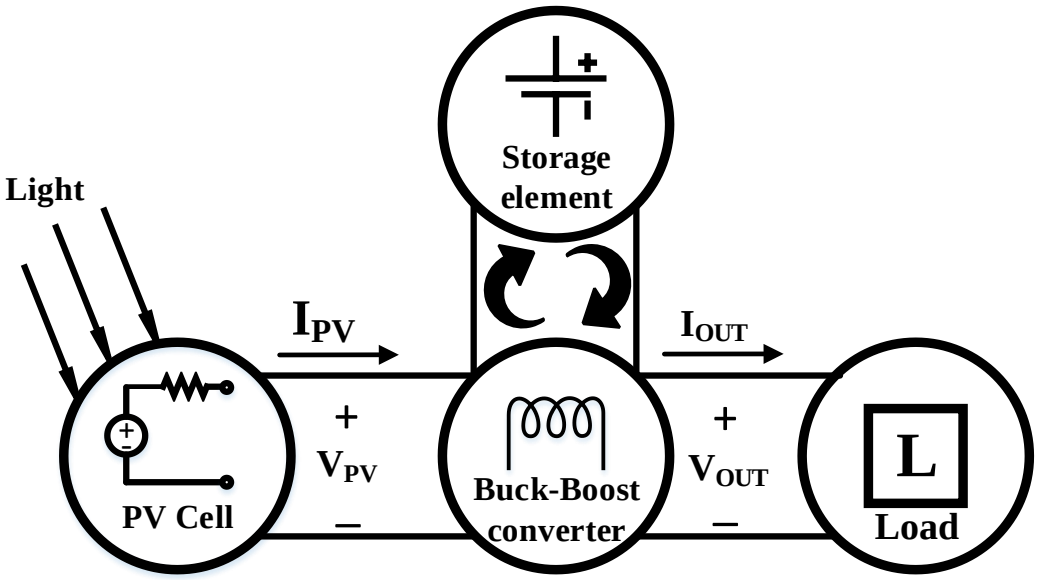

Figure 1.11 Light energy harvesting system including DC-DC converter

element's voltage has to be increased or decreased depending on its state. When the supply voltage is lower than the storage element voltage or the load nominal voltage, a boost converter is needed to step-up the voltage.

Maximum Power Point Tracking (MPPT) is an algorithm used to extract maximum power from a PV module as the input power varies [19]. There are many methods to track MPP, but three main methods of (a) fractional open-circuit voltage (b) hill climbing and (c) artificial intelligence are used in light energy harvesting circuits. In this work, the open-circuit voltage MPPT method is utilized since this method can readily be implemented and has a very low power overhead.

To ensure maximum power point tracking, a control circuit with feedback is needed to track the MPP and deliver power efficiently either to the load or to the storage element. However, the control circuit adds an additional source of power consumption and area

overhead. It also increases the number of component of the energy harvesting system. In this work, a novel energy harvesting system using available resources of a smart sensor is presented which utilizes the sensors MCU instead of control circuits

to perform MPPT and control the distribution of harvested energy between the load and the storage element. Moreover, a new boost-converter circuit is presented for indoor light energy harvesting utilizing MEMS-based switches instead of transistor-based switches to reduce the leakage current and improve the efficiency.

1.5 Research Objectives

Battery maintenance and replacement will be a major issue for a large scale deployment of IoT sensors. The main objective of this research is to explore a practical solution to eliminate the need for batteries to power on IoT sensors.

The research contributions of this thesis have been summarized below:

1. A new energy harvesting method for IoT sensors is presented which utilizes available hardware of IoT sensors to control the process of energy harvesting. This solution reduces the power consumption and lowers the area overhead of the energy harvesting system.
2. A new three switch single inductor boost-converter using MEMS switches instead of transistor-based switches is presented to reduce the leakage current and increase the overall efficiency.

1.6 Thesis Outline

This thesis is organized as follows:

Chapter-I presents a brief overview of energy harvesting methods for IoT sensors and the available ambient sources for energy harvesting in indoor environments. The proposed methods for light energy harvesting is also described in this chapter.

Chapter -II explains the operation of a DC-DC converter in a typical light energy harvesting system and the conventional control methods.

Chapter-III presents a new three switch boost DC-DC converter for light energy harvesting system which utilizes serpentine spring shaped cantilever beam MEMS switches.

Chapter-IV presents a new solution to control a DC-DC converter utilizing available resources of IoT sensors.

Chapter-V presents the conclusion and summarizes the results and future works.

CHAPTER II

BACKGROUND AND RELATED WORKS

Supplying a load with its nominal voltage level by a light energy harvesting circuit in presence of a significant variation of light intensity is challenging. A storage element such as a rechargeable battery or super-capacitor is commonly used in energy harvesting circuits to assists in delivering energy to the load when the harvested energy is not enough to supply the load. The storage element can be charged when the harvested energy exceeds the load requirement. Therefore, a high efficiency and low loss DC-DC converter is needed to distribute power between the storage element and the load. The DC-DC converter is controlled by a circuit to operate in different modes to ensure that the maximum ambient energy is extracted and efficiently delivered to the load or deposited in the storage element.

2.1 Two-Stage Power Converter

A two-stage power converter proposed in [20]-[22] includes two phases of operations, one for MPPT and charging the storage element, and the second for voltage regulation across the load as presented in Figure 2.1. The first stage is used for input impedance matching which is required to deliver the maximum power to the load [23].

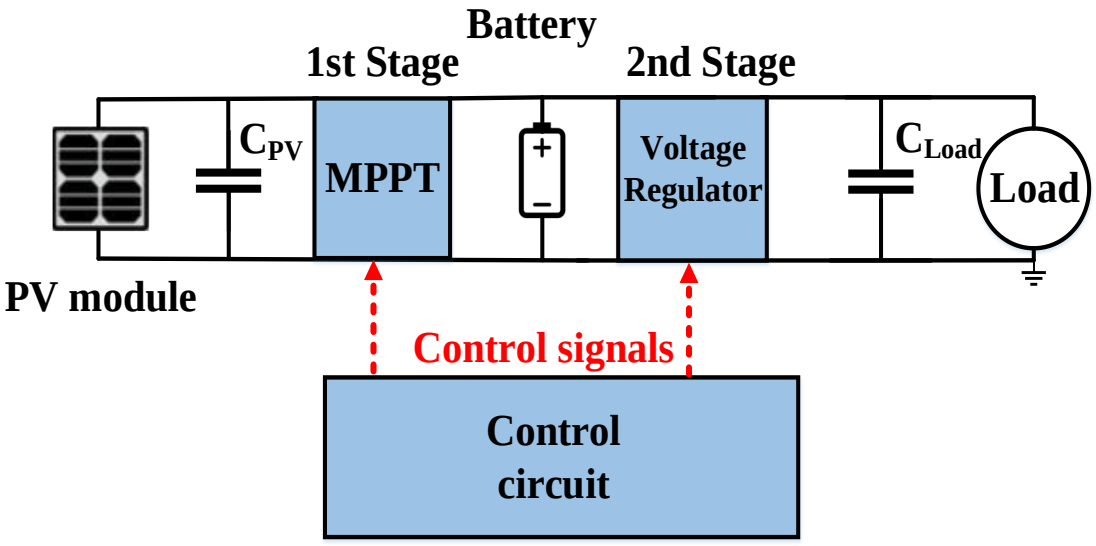

Figure 2.1 Traditional two-stage power converter circuit

The switching frequency of control signals can set the impedance of switched-mode DC-DC converters [23]. This method suffers from power loss since the harvested energy by the PV cell first is delivered to a battery and then to the load. Therefore, the overall efficiency is lower than the efficiency of systems where the energy is directly delivered to the load.

2.1.1 Efficient Two-Stage Power Converter

The two-stage power converter is optimized in [24] where the MPPT stage is divided into two parallel parts as shown in Figure 2.2. The second stage converter operates when the ambient light intensity is enough to directly supply the load. In this state, the energy is delivered to the load by only a single stage power converter. The first power converter is enabled when the voltage across the load falls below a reference voltage, V_{Ref}. When the light intensity is not enough to supply the load, the voltage regulator circuit is enabled to ensure that the load is supplied with the proper voltage level.

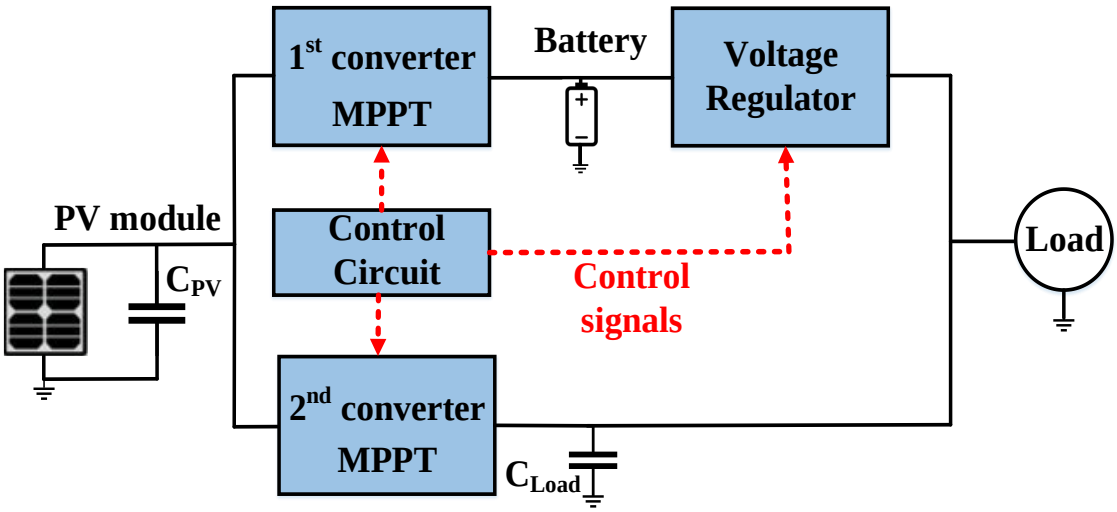

Figure 2.2 Efficient different two-stage DC-DC converter with the control circuit

The gate control signals which are provided by a clocked comparator in the control circuit enables either the first or the second converter. It is reported that this method increases the efficiency by about 12% compared to the dual-path two-stage DC-DC converter [23].

2.2 Single-Inductor Dual-Input Dual-Output Converter

A single-inductor dual-input dual-output with six switches is shown in Figure 2.3. It includes a boost-buck converter with two different paths, one to charge the storage element and the other to supply the load. It can also supply the load directly. The converter monitors the status through two inputs, one from the battery and the other from the PV cell. This converter has been utilized to implement various energy harvesting solution by researchers in [23],[25],[26],[27],[32]. It improves the efficiency over the two-stage converters. However, it suffers from additional power loss due to the number of switches. In order to control the power converter [28] and regulate the load voltage, a relaxation oscillator is used to generate a clock of the system. The energy harvesting system proposed in [29] has

a controller to generate control signals for switches and to compare the voltages. This system reduces the overall cost and increases the efficiency. A PWM signal is generated in the controller to turn on the converter's switches. The controller can change the duty-cycle to regulate the PV cell operating point to track the MPP and ensure that the load is supplied with its nominal voltage level. This solution suffers from additional conduction and switching loss.

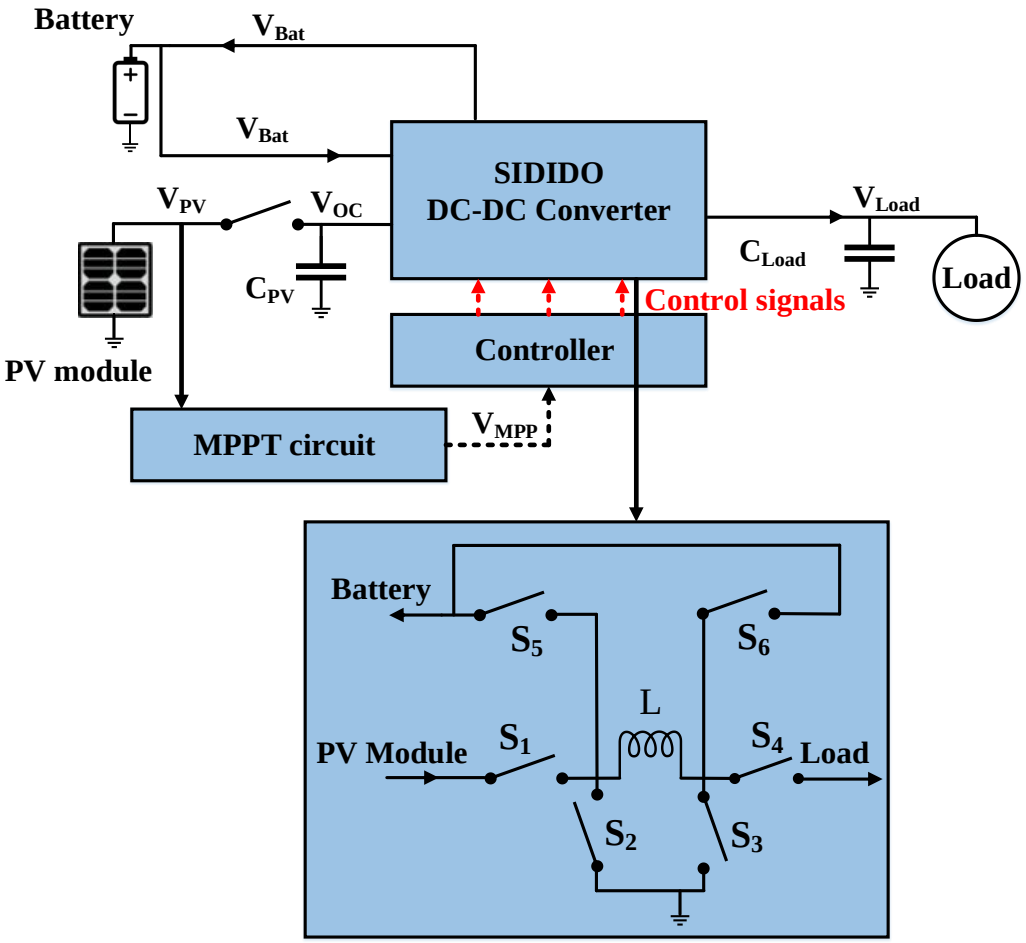

Figure 2.3 A Single-inductor dual path-six switch DC-DC converter

2.3 Dual-Path Three-Switch Single Inductor Dual- Input Dual-Output

The power loss due to the switching reduces the efficiency. Therefore, reducing the number of switches can potentially increase the efficiency. A three-switch single-inductor dual-input buck-boost DC-DC converter is proposed in [30] which consists of one inductor and three switches to harvest energy efficiently with a lower number of switches.

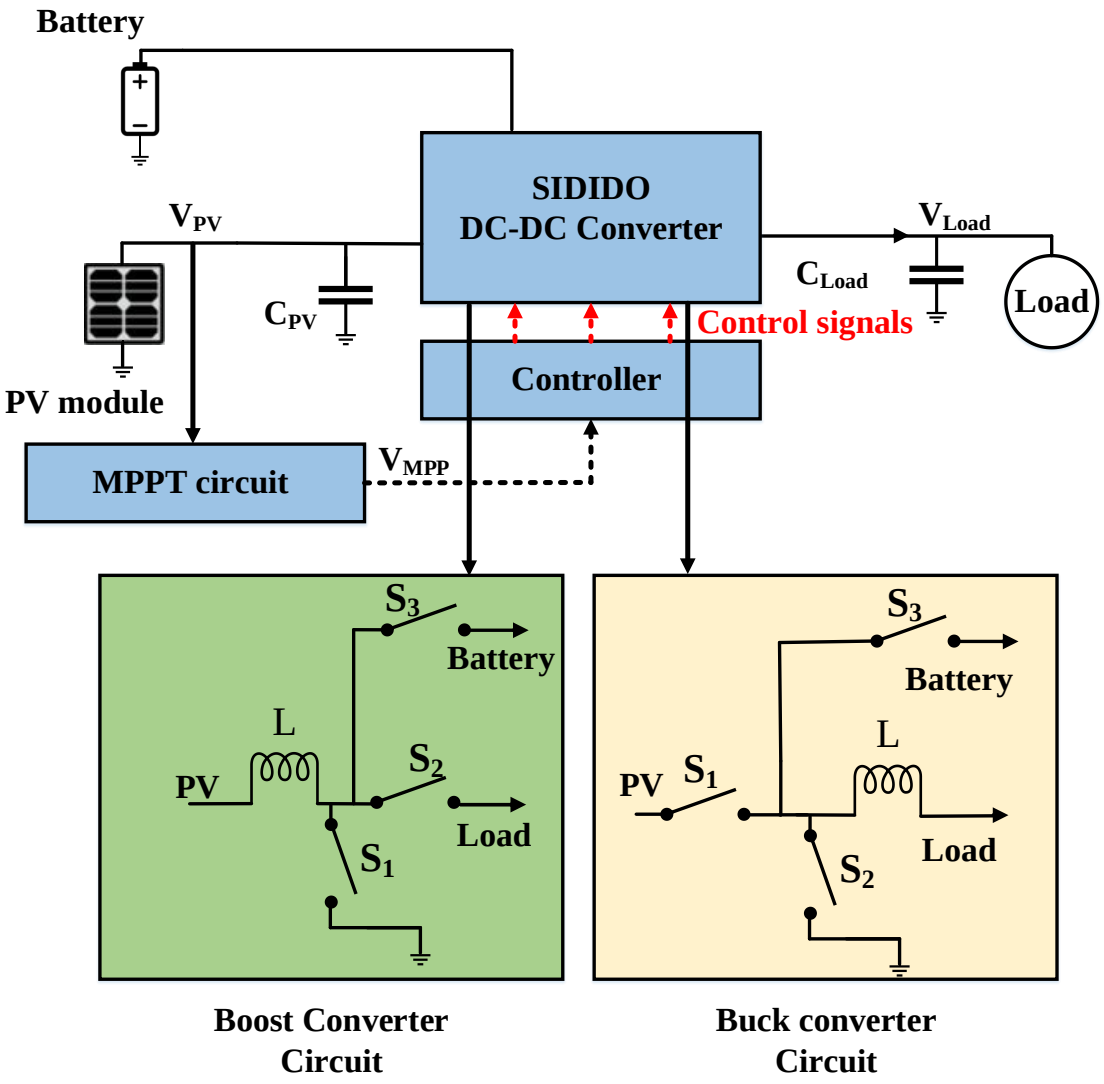

Figure 2.4 Three-switch Dual-path power converter circuit

The design of a three-switch energy harvesting system is presented in Figure 2.4. The system can be used as a boost converter or a buck converter. The boost converter is used to step-up the voltage and the buck converter is used to step down the voltage across the load. The two important factors considered to choose a power converter are (a) the available ambient energy and (b) the sensor load requirements. An energy recycling strategy is proposed in this work which consists of harvest, backup, and recycle modes as indicated in Figure 2.5. When the harvested energy by the PV cell is more than the load requirement, the energy recycling strategy manages the power and delivers the surplus to the battery in the recycling mode.

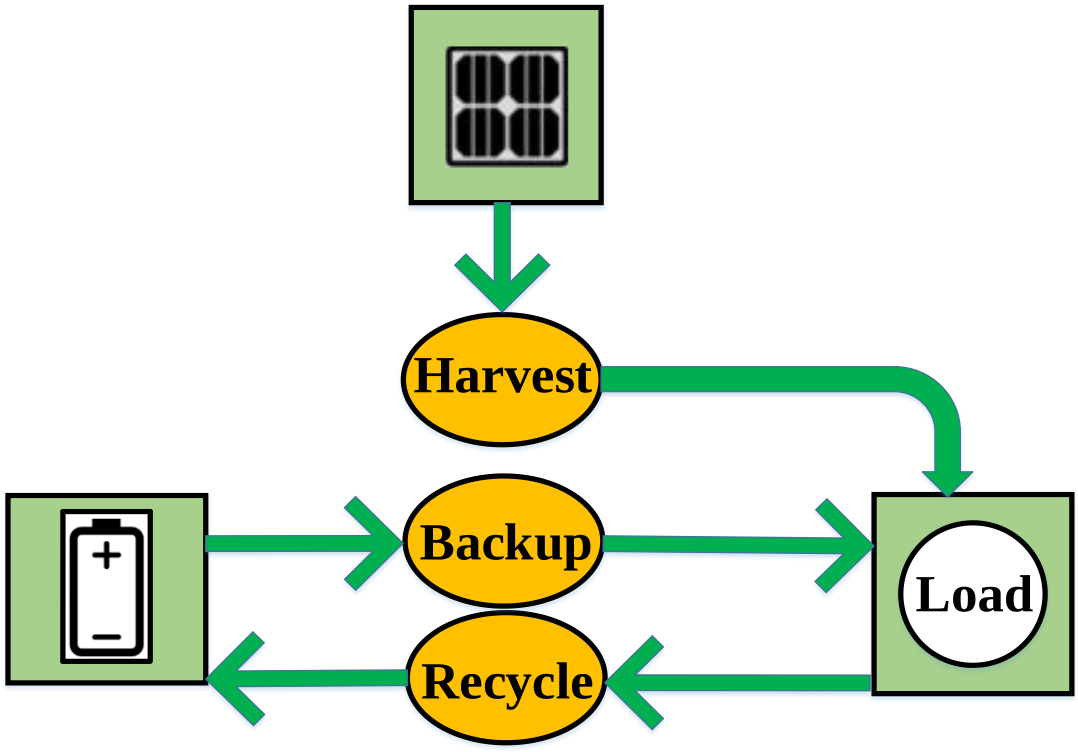

Figure 2.5 The flowchart of three conversion modes in energy-recycling strategy

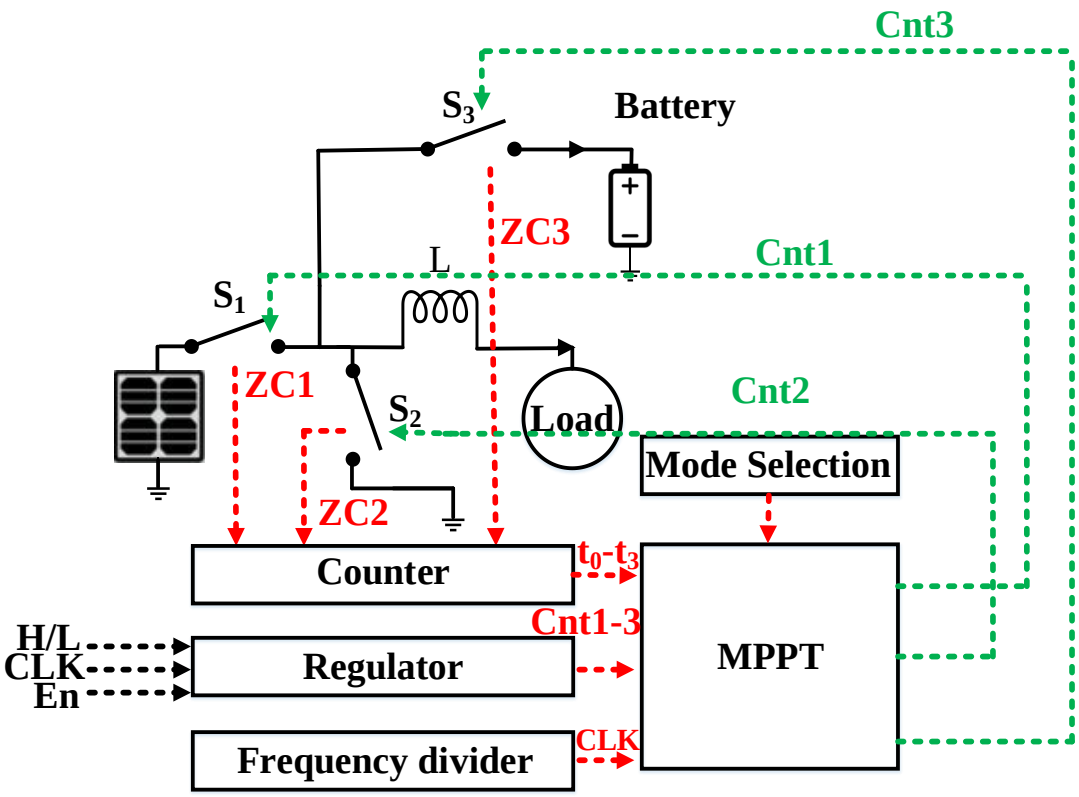

Figure 2.6 Three switch boost converter circuit connected to the control parts

When the light intensity is not enough to power on the load, the PV module and the battery supply the load simultaneously in the backup mode. In order to decrease the power loss in the recycle mode, the size of switches has been optimized, and consequently, the area of the chip is decreased. The efficiency of 93% is reported in this work [30]. This energy harvesting system cannot be readily used in locations where the light intensity is low due to the minimum V_{PV} requirement which has to be 1.8V [31]. In order to solve this problem, a three switch topology based on a boost converter is proposed in [31] which is shown in Figure 2.6. A time-based MPPT is presented in this work to improve the efficiency. The load voltage is regulated by a band-band (hysteretic) control technique. When the load voltage exceeds the upper bound, S_2 turns off to regulate the load voltage. When the load

voltage is between the lower and the upper bound, the PV module can supply the load and when the load voltage falls below the lower bound the PV module cannot supply the load. In this case, the battery is used to power on the load and the converter mode changes from the light-load mode to the heavy load mode. The process of monitoring extracted energy by the PV module is performed by counters in the digital unit. This design can operate in environments with a light intensity as low as 60 Lux and supply the load with 0.5V. It is reported that it can achieve 91.23% efficiency at 470µW.

CHAPTER III

BOOST CONVERTER CIRCUIT USING MEMS SWITCH

3.1 Introduction

Transistor-based switches with different sizes are commonly used in DC-DC converter circuits, but as reported in [33] they present design challenges like leakage current and additional power dissipation especially when the switches are in the standby mode.

3.2 Micro Electro Mechanical System (MEMS) Switch

The rapid development of MEMS technology has enabled the use of MEMS-based devices in many applications. A MEMS switch has advantages over transistor-based switches as it does not present nonlinearities associated with transistor-based switches. A MEMS switch presents a very low ON resistance and a high isolation at the OFF state. MEMS switches consume a negligible amount of power and present a low level of intermodulation distortion which can improve the efficiency [34]. MEMS switches are enabled by electrostatic force and their power consumption are relatively low. The isolation of a MEMS switch is high when the switch is off, and its insertion loss is very low. Table 3.1 shows the comparison between a MEMS switch and conventional switches [35] where $FOM=R_{ON}*C_{OFF}$.

Table 3.1. The comparison between MEMS switch, FET, mechanical, and PIN [35]

	Mechanical	**FET**	**PIN**	**MEMS**
FOM	0.073	270	110	2.5
Isolation	High	Low	Medium	High
Size and weight	Large	Small	Small	Small
Power Consumption	0	0	10mW	0

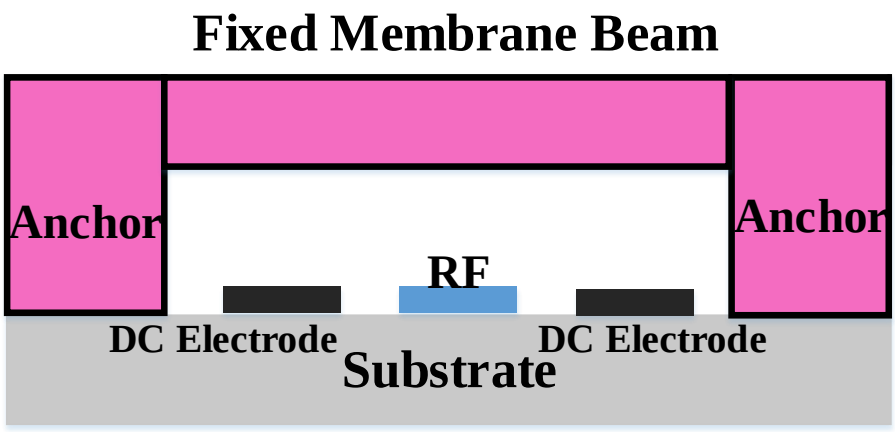

Figure 3.1 Conventional fixed-fixed membrane switch

There are different methods to implement a MEMS switches, the two common MEMS switches are described below.

3.2.1 Fixed-Fixed Membrane Switch

The beam in fixed-fixed membrane switch is fixed to two anchors on both sides as shown in Figure 3.1. There are two actuation electrodes which are located on the substrate and the RF line located in the middle of the substrate. When the voltage is applied to the DC electrodes, the beam deflects and connects to the RF line. The fixed beam remains in its steady state without any deflection when a voltage is not applied to the switch.

3.2.2 Cantilever MEMS Switch

Many studies have been conducted to develop a Cantilever MEMS switch in different shapes [36][37][38]. A cantilever beam MEMS switch is shown in Figure 3.2 which indicates that the cantilever beam is connected to an anchor that is fixed to the substrate from one side. Figure 3.2 (A) shows the switch in the OFF state. Figure 3.2 (B) indicates the status of the switch when it is activated by an applied voltage to the DC electrode. The RF lines are conductive materials such as Gold or Aluminum to ensure a low ON resistance [35]. Figure 3.2 (C) shows the equivalent circuit of a MEMS switch in both ON and OFF states. When the switch is off, it acts like a capacitor, and when the switch is ON it behaves like a resistor.

3.3 Advantages of MEMS Switch Over Transistor-Based Switch

A transistor-based switch presents an ON resistance which depends on the input voltage. To minimize the ON resistance two large size NMOS and PMOS transistors are commonly used to implement a switch. Such a configuration presents a significant parasitic capacitance and suffers from a considerable leakage current in the OFF state. In a MEMS switch the leakage current in the OFF state is almost zero and in the ON state its resistance is negligible. The airgap in a MEMS switch creates a low off-state parasitic capacitance and a high isolation compared to the transistor-based switches. Transistor-based switches are non-linear devices and have intermodulation distortion, but a MEMS switch is a linear device and presents a very low intermodulation distortion [39].

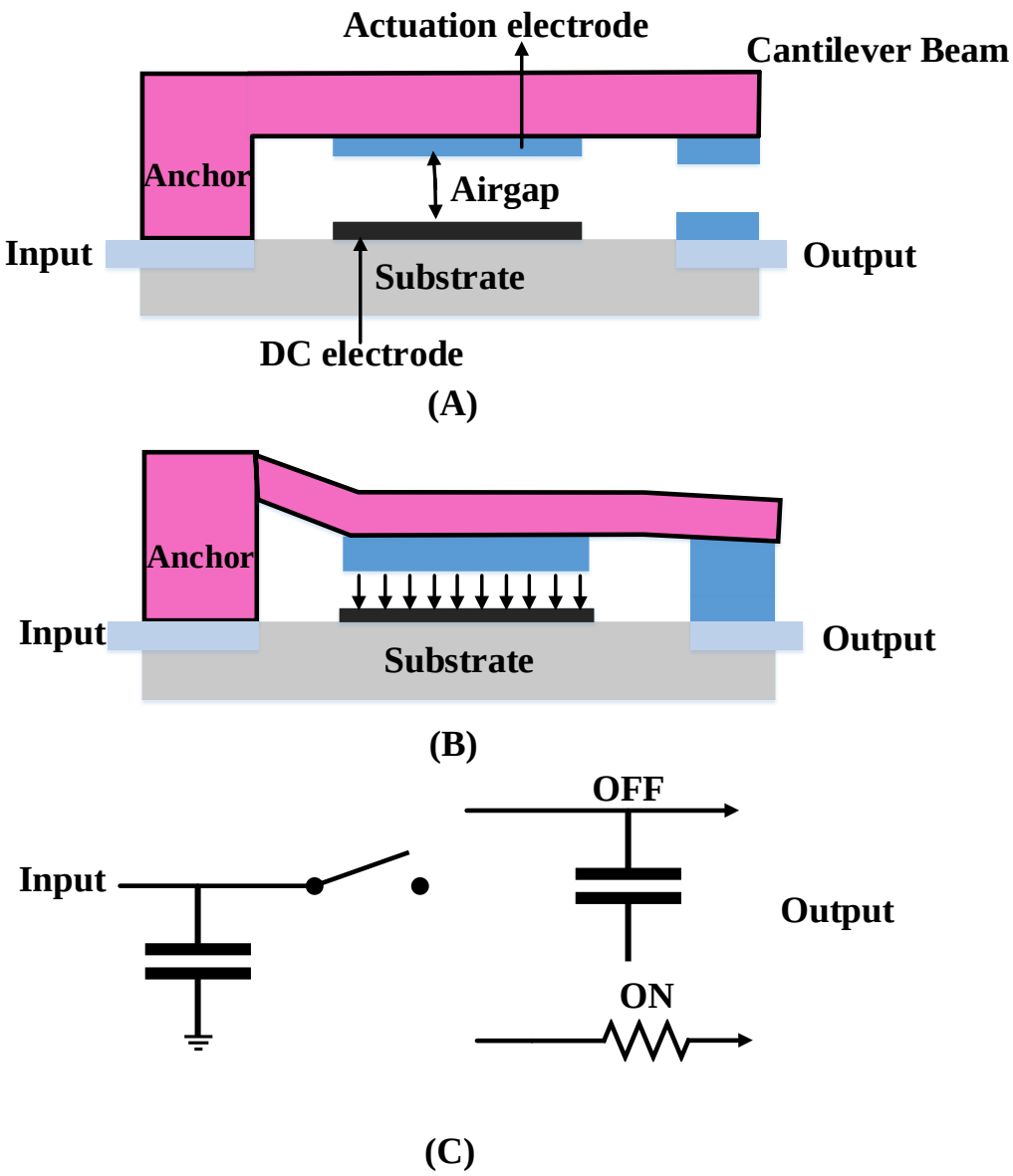

Figure 3.2 (A) Cantilever MEMS switch when it is in open (OFF) state, and (B) is the cantilever switch when it is in closed (ON) state. (C) Equivalent circuit of the cantilever MEMS switch in ON and OFF state

3.4 Disadvantages of MEMS Switch Over the Transistor-Based Switch

MEMS switches have a lower speed compared to the transistor-based switches, and therefore they are not suitable for high-speed applications such as radar systems [39]. The ability of power handling of MEMS switch was the weakness of MEMS switches in past

but practical solutions have been proposed to improve the power handling of these devices [40][41][42][43].

The packaging cost of MEMS switches is high compared to the integrated circuits because the environment needed for MEMS packaging should have a very low humidity, and filled with nitrogen. MEMS switches require a relatively high actuation voltage, but studies have been conducted to decrease the actuation voltage of these devices by reducing the spring constant or increasing the actuation pad area [39].

3.5 Using MEMS Switch for Energy Harvesting Applications

Cantilever MEMS switches are used for many applications due to their advantages. A Cantilever MEMS switch can be designed to work with a low-actuation voltage.

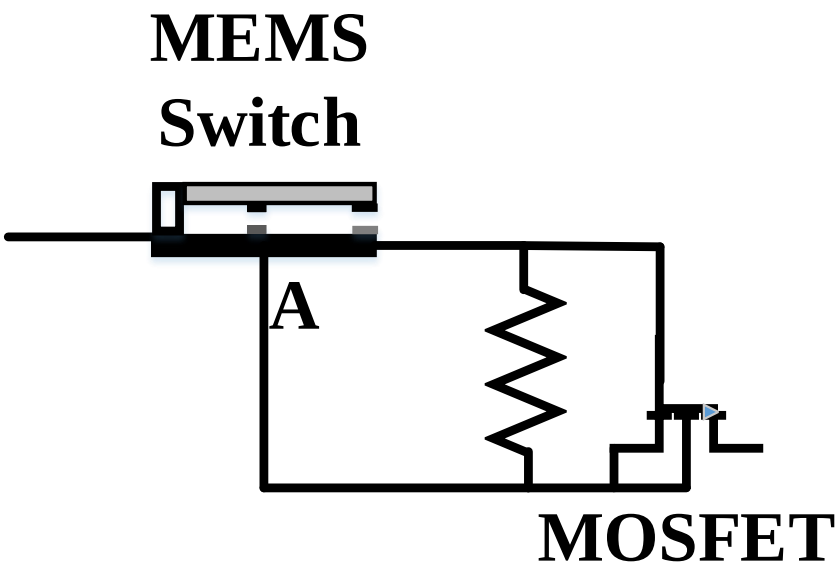

Figure 3.3 Using MEMS switch as a gate driver of a MOSFET

A cantilever MEMS switch is utilized in [44] which is used as a gate driver of a MOSFET switch as shown in Figure 3.3. When the voltage between point A and the cantilever beam increases and the electrostatic force exceeds the spring's elastic force, the cantilever beam is pulled down and the MEMS switch turns on. Then the input voltage is applied to the gate of a MOSFET transistor. However, when the voltage decreases below a certain amount, the cantilever beam returns back to its previous state, and the gate to source voltage falls to zero volts [44]. This MEMS switch is used for energy harvesting system, but it needs 12V actuation voltage which is considered a high voltage for such an application. A low-actuation voltage of 4V is reported in [45] for a serpentine shape cantilever switch. In [46] the size of the switch is shrunk and small holes are created on the upper electrode of the cantilever beam to reduce the actuation voltage.

In this work, a cantilever type MEMS switch is designed for the power converter circuit. A cantilever of serpentine shape is designed to reduce the pull-in voltage to ensure its operation in indoor environments. The proposed solution decreases the leakage current and reduces the loss of energy due to the switching activities.

3.6 The Proposed Power Converter Circuit Using MEMS Switch

The schematic diagram of a three-switch boost-converter utilizing MEMS switches is shown in Figure 3.4. The proposed energy harvesting system consists of a PV cell, three

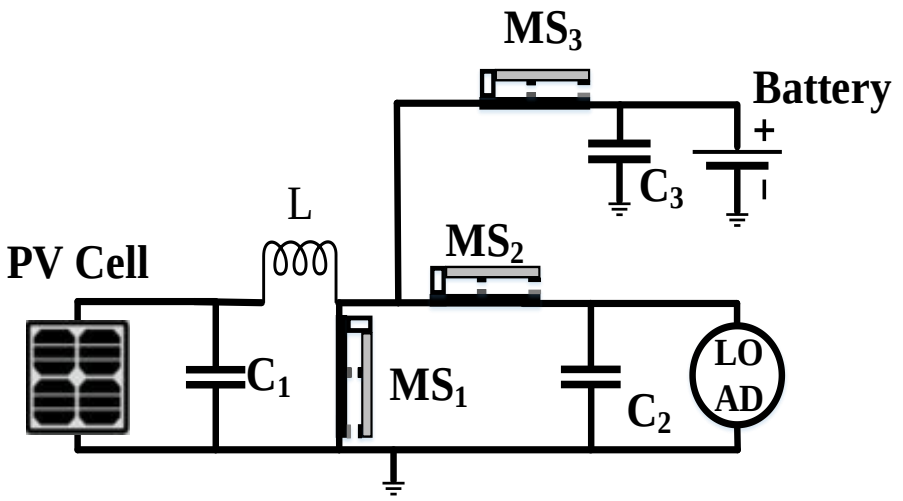

Figure 3.4 Schematic of three switch boost converter circuit implemented using MEMS switches

MEMS switches, a battery, an inductor, and three capacitors used to reduce the ripple in the charging and discharging states [31]. The energy harvested by a PV cell is delivered to the load through MEMS switches. When the harvested energy is more than what is needed by the load, the energy surplus is stored in the battery. When the light intensity is not adequate, the battery assists the PV cell to supply the load through a switching cycle to turn ON and OFF the MEMS switches in appropriate time slots.

The proposed circuit operates in both recycle and backup modes which are described in chapter II. When the light intensity is high the circuit works in the recycle mode. When the voltage across the first MEMS switch exceeds the threshold MS_1 is turned on and the charge accumulates in the inductor. When the DC electrode voltage of MEMS switch falls

below the threshold, the cantilever pulls up and MS_1 turns off. Then SM_2 is closed and the energy stored in the inductor is transferred to the load. In the third step, MS_3 is activated and the excess energy in the inductor is used to charge the battery. If the boost converter circuit is designed with transistor-based switches, the amount of power loss caused by the static and dynamic power consumption of transistor switches will reduce the efficiency. The mode transition from the recycling-mode to the backup mode and the switching cycles consumes power and reduce the efficiency [47].

If the amount of leakage current in transistor-based switches is taken into consideration in the recycle mode with three switching cycles, the surplus charge packet which is transferred to the battery is calculated from:

$$P_{Battery} = \frac{1}{2}L\left(\Delta I_L - I_{Leakage}\right)^2 - (P_{Load})\Delta T \tag{3-1}$$

where ΔT denotes the on time for MS_3, ΔI_L is the inductor current variation, L is the inductance, $I_{Leakage}$ is the subthreshold leakage current, P_{Load} is the power consumption of the load, respectively. The subthreshold leakage current is calculated [47] from:

$$I_{Leakage} = (\mu C_{ox}\frac{W}{L}(\frac{KT}{q})^2 e^{1.8}) * e^{\frac{(V_{gs}-V_{th})}{n\frac{KT}{q}}}\left(1 - e^{\frac{-V_{ds}}{\frac{KT}{q}}}\right) \tag{3-2}$$

where V_{gs} is the gate to source voltage, V_{th} is the threshold voltage, V_{ds} is the drain to source voltage, and n is the subthreshold swing coefficient. T is the temperature, q is an electron charge, and K is Boltzmann constant. C_{ox} is the gate oxide capacitance, and μ is the zero bias mobility. W and L represent the width and length of the transistor.

When the harvested energy is not enough to supply the load, the control circuit changes the mode of the converter to the backup mode to turn on SM_3 to charge C_1. When C_1 is charged, SM_2 and SM_3 are turned on respectively similar to the sequences in the recycle mode to supply the load. If the energy harvesting system remains in the backup mode, the power loss of transistor switches may deplete the remaining energy, and consequently turn the system off. The energy which is delivered to the load is a combination of energy from the battery and the PV cell which is:

$$P_{Load} = \left(P_{Battery}\right)\Delta T + \frac{1}{2}L\left(\Delta I_L + I_{Leakage}\right)^2 \quad (3\text{-}3)$$

where $I_{Leakage}$ is the leakage current of MS_1, $P_{Battery}$ is the power of the storage element. The lack of leakage current in MEMS switches which is due to the very high isolation makes them suitable for energy harvesting applications.

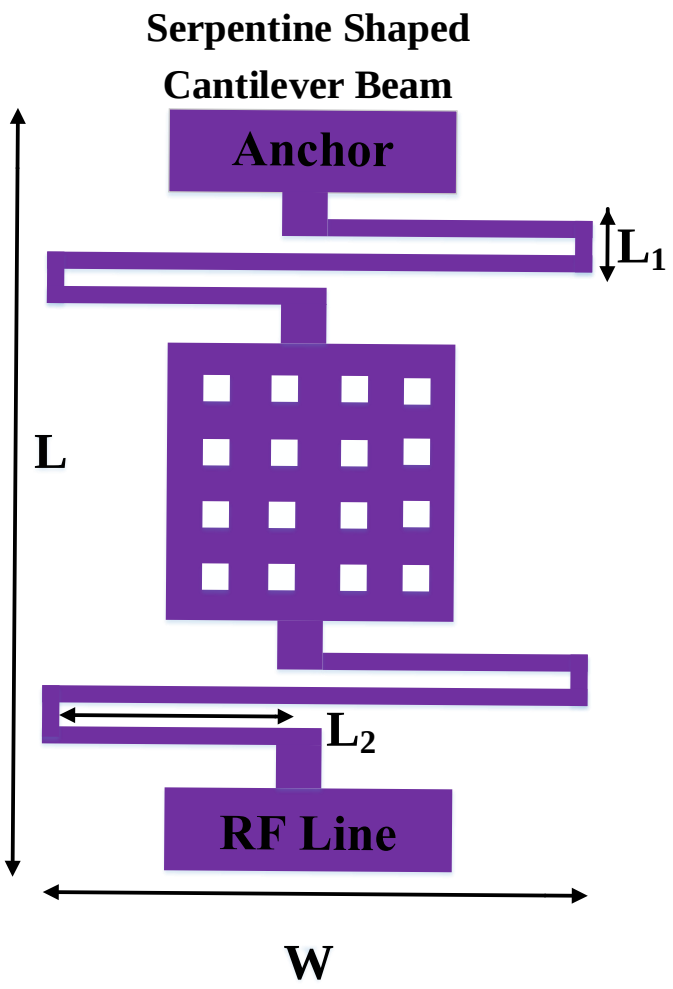

Figure 3.5 Top view of the designed MEMS switch

3.7 Proposed MEMS Switch

A serpentine shape MEMS switch is designed in this work. The top view of the switch is shown in Figure 3.5. This MEMS switch includes an anchor on the left side of the structure which holds the cantilever beam. The cantilever beam consists of four meander type beams which can reduce the spring constant, and the designed holes on the upper electrode of the beam significantly decrease the beam mass, extra stress, and resonant frequency [48]. The MEMS switch is designed with parameters and materials specified in Table 3.2. The parameters are calculated to have a low actuation voltage which makes the switch more

compatible with indoor energy harvesting systems. The actuation voltage depends on some parameters as described by the following equation:

$$V_{Pull-in} = \sqrt{\frac{8K_Z g^3}{27W\varepsilon_0}} \tag{3-4}$$

Where W is the pad area of the input and output (Actuation area), g is the air gap between the gate electrode metal and the beam metal, ε is the air permittivity, and k_z is the spring constant.

The pull-in voltage is depended on some parameters as shown in the equation (3-4). The cantilever beam is pulled down by the electrostatic force caused by the voltage applied to the actuation electrode. The electrostatic force, F, is calculated from:

$$F = \frac{\varepsilon_0 W V_{Pull-in}^2}{2(g_{in}-d)^2} \tag{3-5}$$

Where W is the area of DC electrode, $V_{Pull\text{-}in}$ is the applied voltage to the bottom electrode, g_{in} is the initial gap between the upper and the bottom electrode when there is no displacement, and d is the displacement between the cantilever and the bottom electrode. The pull-in voltage is proportional to the spring constant of the structure, K, air gap. In this work, the dimensions of MEMS switch have been optimized to achieve a higher pad area to reduce the pull-in voltage.

Table 3.2 MEMS switch dimensions and required material constants

Parameter	**Values**
Substrate	525×300 μm
Anchor	60×150 μm
Primary meander length (L1)	30 μm
Secondary meander length (L2)	160 μm
Beam Width (w)	300 μm
Switch thickness (t)	1.5 μm
Air gap	0.5 μm
Young's modulus of Gold (E)	57GPa
Poission's ratio of Gold	0.35
Z-axis moment of inertia (I_z)	tw^3/12
X-axis moment of inertia (I_x)	t^3w
Torsion modulus (G)	E/2(1+v)
Torsion constant (J)	I_p × 0.413
Polar moment of inertia (Ip)	I_x+I_z
Actuation electrode area	150×150 μm

The flexibility of the cantilever beam is depended on its spring constant, which is basically the stiffness of the cantilever beam. The spring constant of the proposed structure is calculated [45] from:

$$K_z = \left[\frac{(512{L_1}^3)+8{L_2}^3}{3EI_x} + \frac{4L_1L_2[3L_2+153L_1]}{3GJ} - \frac{4{L_1}^2\left[\left(\frac{8L_1}{EI_x}\right)+\frac{9L_2}{GJ}\right]^2}{2\left(\frac{L_1}{EI_x}+\frac{L_2}{GJ}\right)} - \frac{4{L_2}^3}{2}\left(\frac{L_1}{GJ}+\frac{L_2}{EI_x}\right)\right]^{-1} \quad (3\text{-}6)$$

where L_1 is the primary meander length of the beam, L_2 is the secondary meander length, J is portion constant, and G is the torsion module.

The proposed MEMS switch is designed and simulated in Intellisuite software as shown in Figure 3.6. The switch is designed with an air gap of 0.5μm in 3D builder module of Intellisuite. Figure 3.6 (A) shows the top view of the designed MEMS switch and Figure 3.6 (B) shows the cross view of the switch when it is open. The two blue parts show the

RF contacts, the green electrode shows the DC electrode which is covered by a Si3N4. Figure 3.7 shows the cross view of the MEMS switch when it is closed.

3.7.1 Material Selection of the Proposed MEMS Switch

Gold is usually used to build a MEMS switch beams because of its inherent stiffness and flexibility. Gold supports a good mechanical performance when the beam deflects to close the switch and when it pulls up to return to its initial position. Moreover, gold has a low resistance and it is resilient against corrosion. A layer of silicon nitride is deposited on the top layer of actuation electrode as a sacrificial layer in order to avoid a short circuit between the gold beam and the actuation electrode [36].

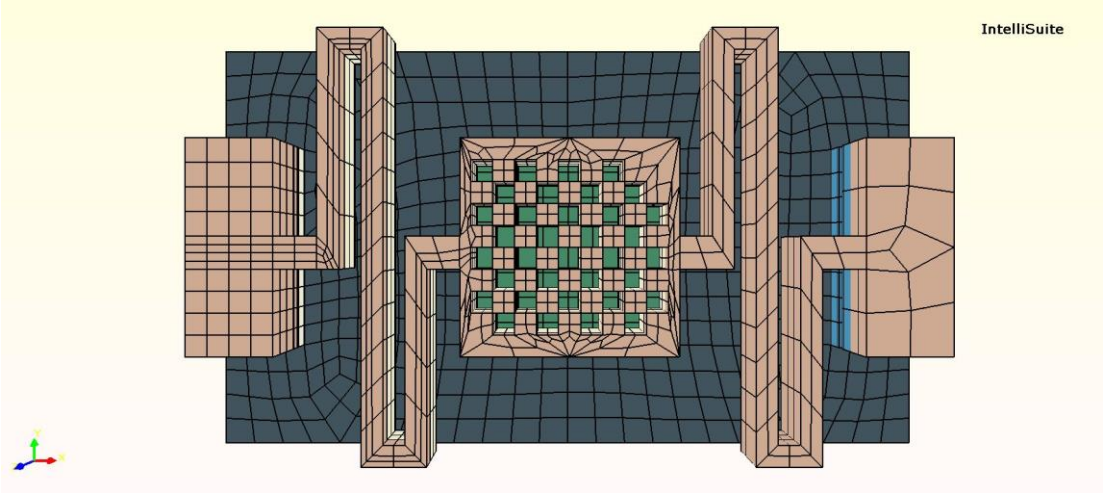

(A)

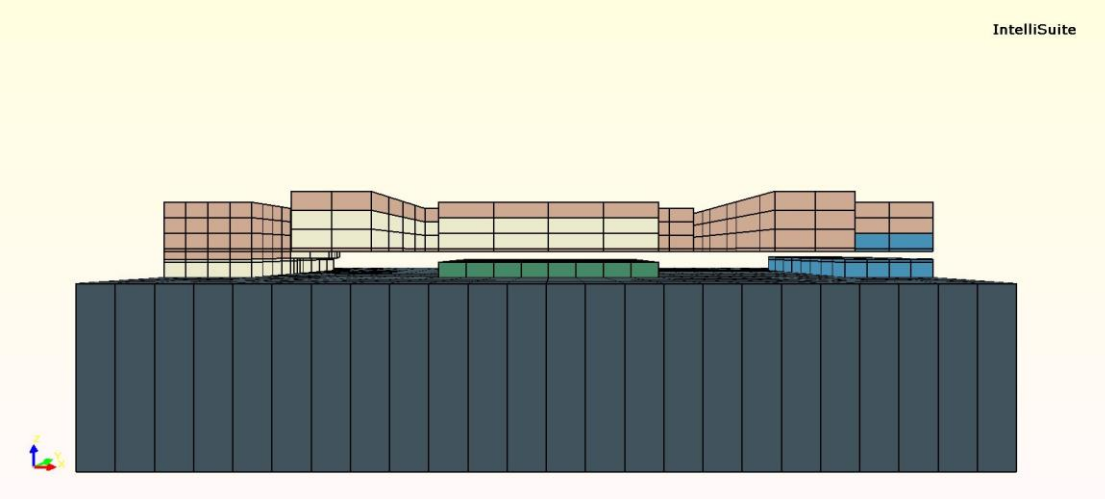

(B)

Figure 3.6 (A) The top view of designed MEMS switch in Intellisuite software (B) The cross view of MEMS switch in OFF state

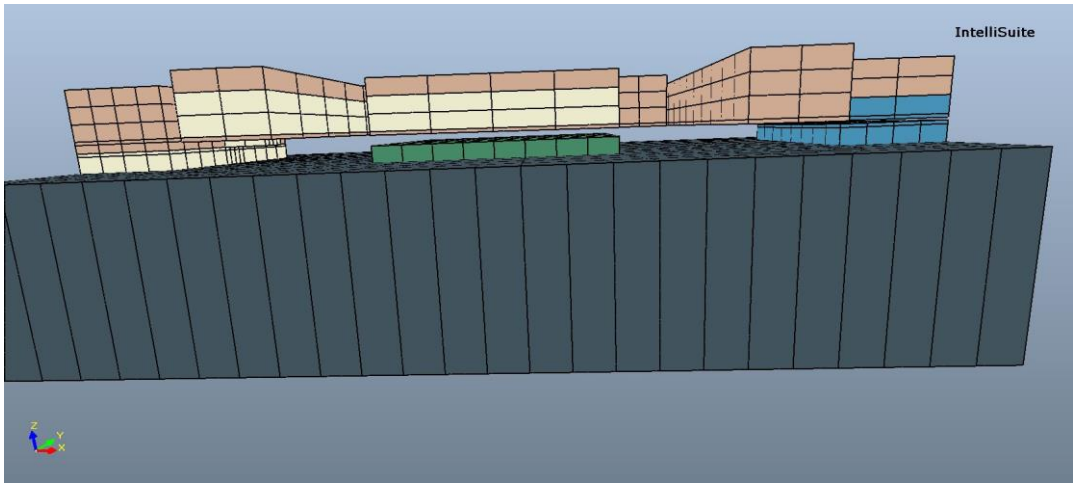

Figure 3.7 The cross view of MEMS switch when in ON state

3.7.2 Simulation Results

The designed serpentine shape MEMS switch in 3D Builder is exported to ThermoElectroMechanical (TEM) module of Intellisuite for static analysis. The building materials are selected for different parts of the switch as mentioned in section (3.7.1). The substrate and the anchor are fixed by applying the boundary condition. The static analysis has been performed to demonstrate the displacement of the designed switch in Z-

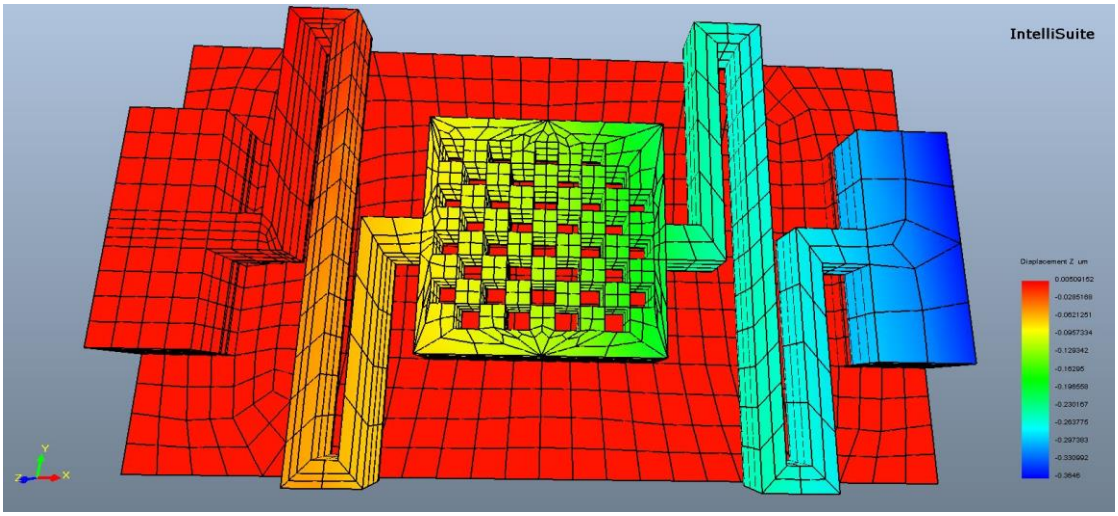

Figure 3.8 The displacement result of static analysis in Z-axis

axis. The result of displacement is shown in Figure 3.8. The simulation result represents that the upper RF line has higher displacement compared to the other parts of the switch with deflection of 0.364μm.

The pull-in voltage of MEMS switch is calculated from equation (3-4). To get the pull-in voltage via the simulation, the voltage applied to the contact varied from 0 to 1V to perform TEM simulation. The results in Figure 3.9 represent the displacement in the Z-direction with the applied voltage.

The equivalent circuit of the MEMS switch with the same characteristics is used to create a switch in Cadence environment to perform simulations. A three-switch power converter circuit utilizing MEMS switch is implemented in Cadence Virtuoso design environment. The same circuit is also implemented with transistor-based switches as shown in Figure 3.10.

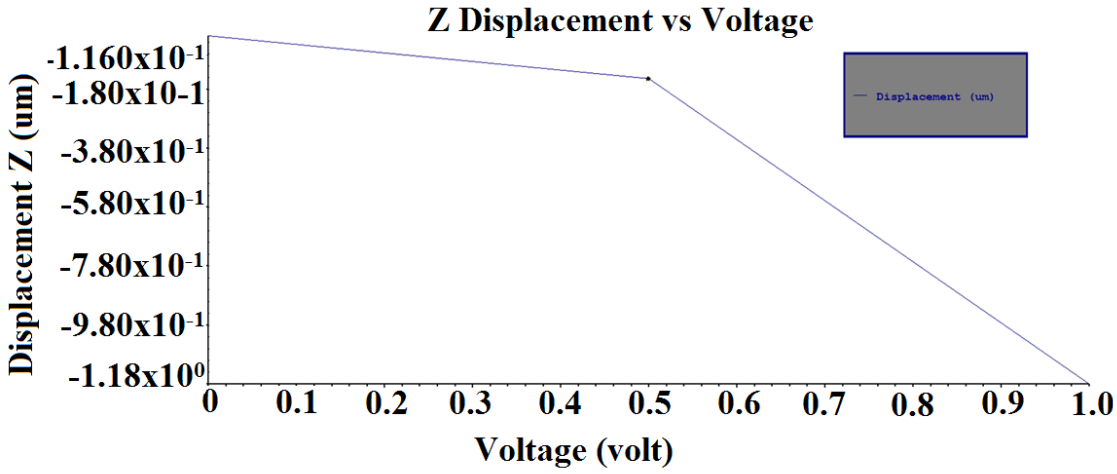

Figure 3.9 Beam Z-displacement versus voltage

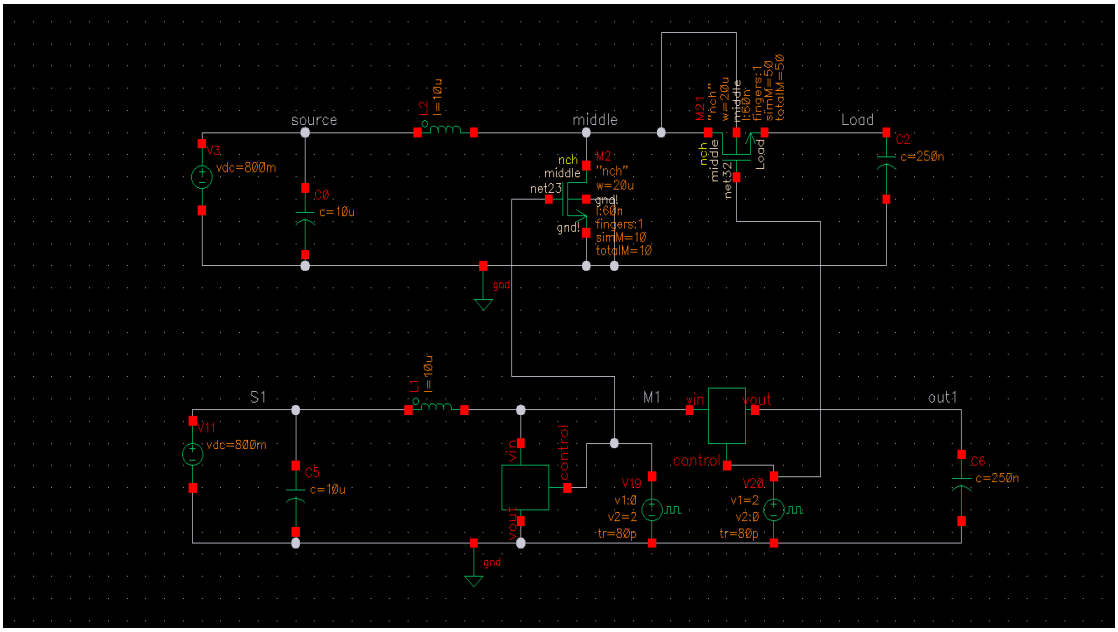

Figure 3.10 The schematic diagram of the three-switch boost converter in Cadence environment

The simulations were performed with the 800mV input voltage. The results in Figure 3.11 show that the output voltage of the converter using MEMS switches is higher than the output voltage of the same circuit using transistor-based switches.

The load voltage level, V_{Load}, after 10 cycles are measured for both circuits and then the harvested energy calculated from $1/2C\Delta V^2$. The boost converter circuit with the MEMS switches presents 17% higher efficient than the circuit with transistor-based switches.

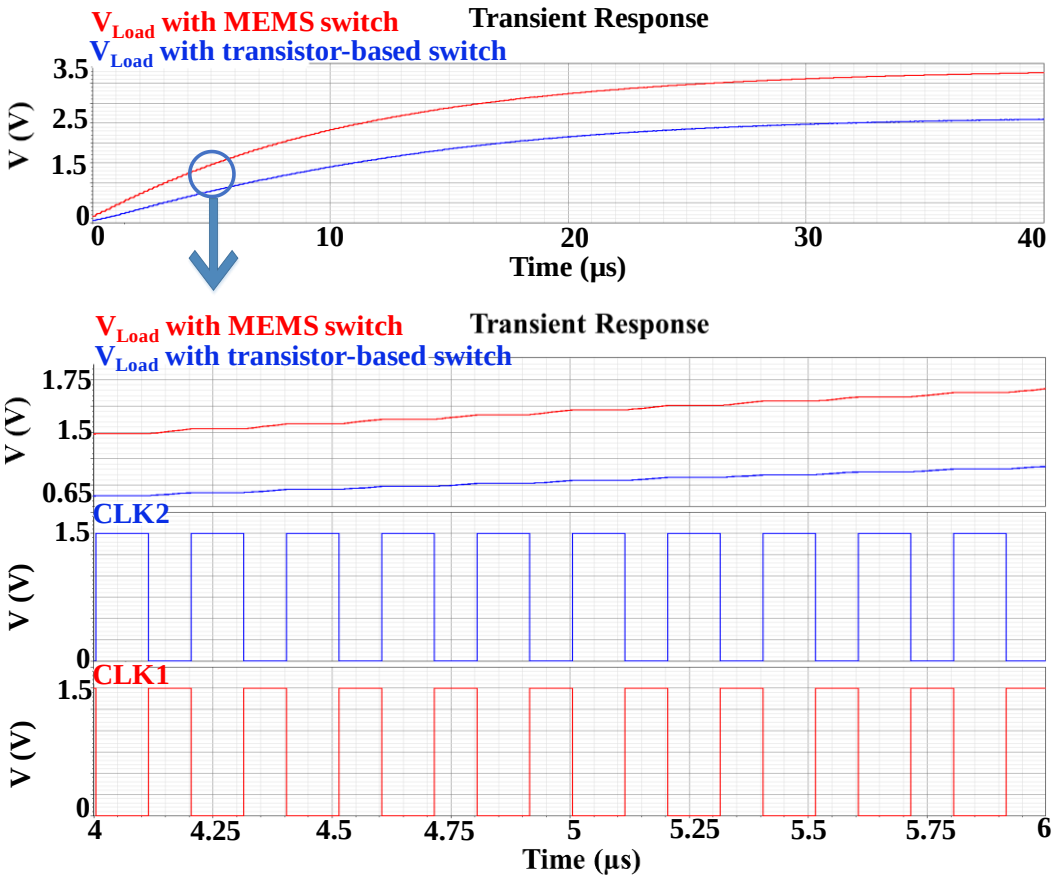

Figure 3.11 Simulation results of the proposed power converter circuit with transistor-based switches and MEMS switches

3.8 Conclusion

A serpentine shape cantilever MEMS switch is designed using Intellisuite software with a low actuation voltage. An equivalent circuit model for the switch is used to perform simulations in Cadence design environment. A three-switch single-inductor boost converter circuit was implemented to perform simulations. The simulation results in the recycle mode of the boost converter indicate that using MEMS switches instead of transistor-based switches reduces the power loss and enhances the efficiency of the system by about 17%.

CHAPTER IV

DIGITALLY CONTROLLED BOOST CONVERTER CIRCUIT FOR INDOOR LIGHT ENERGY HARVESTING SYSTEM

4.1 Introduction

As mentioned in chapter II, various DC-DC converters are proposed in the literature with different control strategies, but they need additional control circuits which increases the cost and reduces the efficiency.

IoT wireless sensors are designed for low power applications. Most of the available IoT sensors in the market include an MCU which is optimized to consume low power. The MCU has all the required resources to control an energy harvesting circuit. The reuse of MCU to follow MPPT algorithms for energy harvesting can reduce the costs and improves the energy harvesting efficiency. In [49] a perturb and observe algorithm to track the maximum power point is presented using an ARM-Cortex which consists of an ADC and PWM unit. The voltage and the current are measured in this method by an ADC and then the data are sent to the software to track the MPP. A buck converter implemented with one switch is proposed in [50] which works with a clock signal of 25KHz to step down the voltage from various voltage level to 9V. The switches are controlled through PWM generated by the MCU. A gate driver circuit is implemented at the output of the MCU to increase the amplitude of the PWM to drive a MOSFET gate.

In this work, a new control algorithm is presented for a four-switch single-inductor dual-path boost converter using the available MCU on Texas Instrument's sensor tag. The

proposed algorithm decreases the area occupied by the control circuits in the energy harvesting system by controlling the energy harvesting process through an algorithm implemented in the sensor's firmware. The proposed design is suitable for indoor applications and can work with a light intensity as low as 200 Lux. The proposed energy harvesting circuit is fabricated on a PCB board and connected to a sensor tag for evaluation.

4.2 TI Sensor Tag Power Requirement in Various Sensor's Operation

The CC2650 TI sensor tag is a wireless sensor with an embedded CC2650 MCU that can communicate using BLE. This device is a low-power sensor that can operate for almost a year with a 3V lithium coin battery if it is used properly. The main CPU of the sensor is a 32-bit Cortex-M3 processor as shown in Figure 4.1. The general peripherals and sensor controller parts of the MCU consists of multiple timers and an ADC [51].

The power consumption of the sensor when it is in the standby mode in 3μW. In this mode, the timer works to detect a wakeup call and change the status to the active mode when it is required. The power consumption of the sensor tag in different modes of operation is summarized in Table 4.1. The maximum power consumption is reported to be approximately 14.4mW.

Table 4.1 Amount of needed power of TI sensortag in Active and Standby modes

Operation mode	**MCU power consumption (P_{MCU})**	**Sensor power consumption (Psensor)**
Standby Mode	3µW	240µW
Active Mode	4.3mW	14.4mW

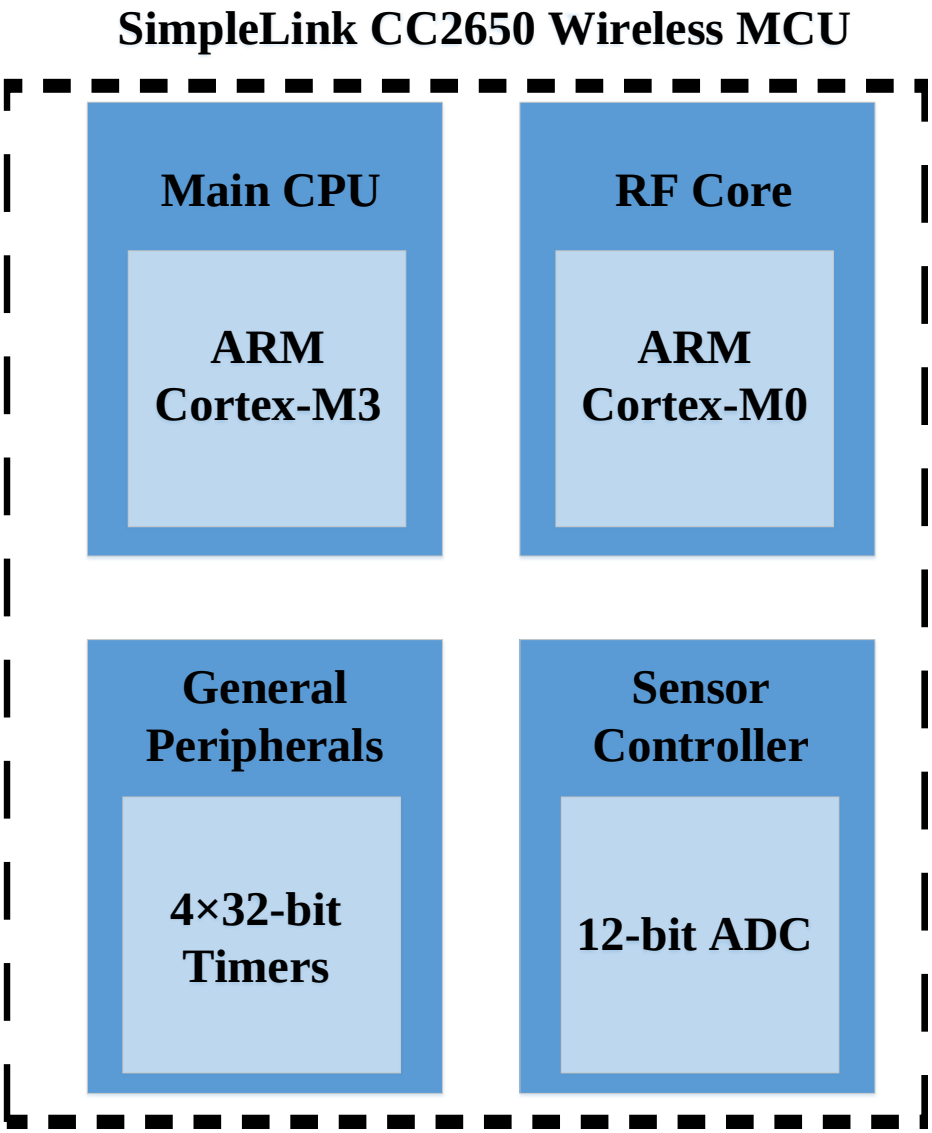

Figure 4.1 Block diagram of CC2655

When the sensor turns on and starts advertising with a maximum speed of 190kb/s, the current consumption becomes approximately 7.47mA [52].

The total current consumption of the sensor, I_{Total} , is given by [61]:

$$I_{Total} = \left(\frac{1}{2}s * \frac{P_{Total}}{V_{Total}}\right) + (t_S * \frac{I_{Sleep}}{t_S}) \quad (4\text{-}1)$$

where P_{Total} is the maximum power consumption of the sensor, V_{Total} is the operating voltage of the sensor, t_S is the wake-up time interval of the sensor, and I_{Sleep} is the current consumption of sensor in sleep mode.

If the duration of the data transmission of the sensor takes $t_{transmission}$, the required current for transmission is calculated from

$$I_{transmission} = \frac{(I_B + I_{MCU-Active}) * t_{transmission}}{t_T} \quad (4\text{-}2)$$

where I_B is the BLE current consumption when it transmits data. I_{MCU} is the MCU current consumption in the active mode. The overall power consumption by the sensor is given by:

$$P_{Overall} = (I_{Total} + I_{transmission}) * V_{Total} \quad (4\text{-}3)$$

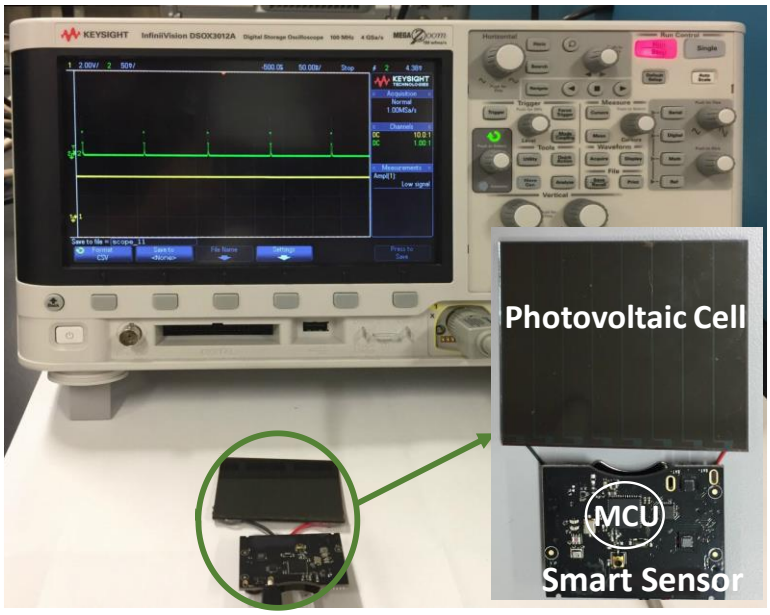

(A)

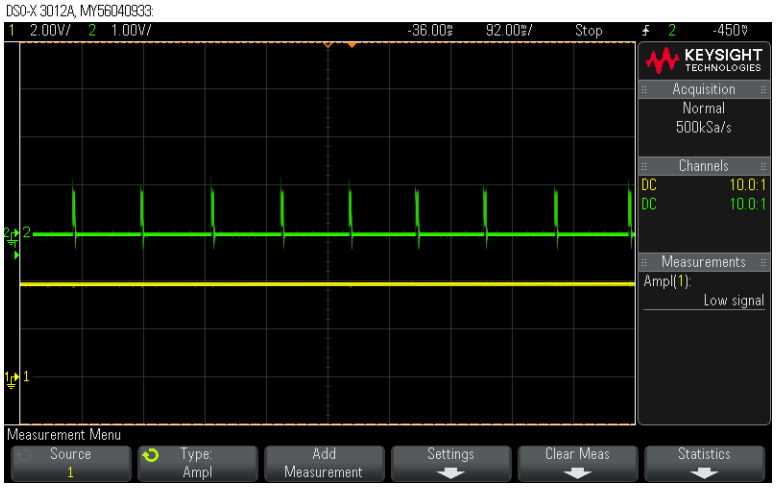

(B)

Figure 4.2 (A) Measurement setup. (B) The supply voltage provided by the PV cell and the operation of the MCU in the active mode time slots

Experiments measurements were performed to determine the required light intensity to ensure that enough energy can be harvested to power on the sensor. Figure 4.2 (A) shows a commercially available sensor connected to a PV module with the dimensions of 58cm × 48cm. Figure 4.2 (B) shows the voltage across the sensor. When the PV is exposed to

about 200Lux light intensity, which is available in most fluorescent illuminated buildings, the sensor PV energy cannot turn on the sensors. If a DC-DC converter circuit is added between the PV cell and the sensor, enough energy can be stored even with 200Lux light intensity to turn on the sensor for a short period of time to communicate.

4.3 The Proposed Energy Harvesting System

A new energy harvesting system shown in Figure 4.3 is designed for the sensor. The power converter is controlled through an algorithm implemented on the MCU firmware. The block diagram of two parts of the MCU connected to the energy harvesting system is indicated in Figure 4.3. The system includes a PV module, a boost converter circuit, a supercapacitor, an ADC, and general peripherals.

The proposed boost converter can operate even with a very low light intensity and can supply the sensor with a constant voltage. The ADC in the MCU is used to monitor the voltage across the PV cell, V_{PV}, and the load, V_{Load} to control the energy harvesting process. Depending on the voltage level, the MCU executes suitable algorithms for operation of the converter circuit. The output the algorithm execution is a PWM signal to control the switching sequence of S_1 to S_4 to either transfer the energy from PV cell to the load or to store the energy in the supercapacitor. The reuse of MCU modules adds the capacity to control the process of energy harvesting through firmware without using any extra control circuit, mode-detection module, and MPPT circuit.

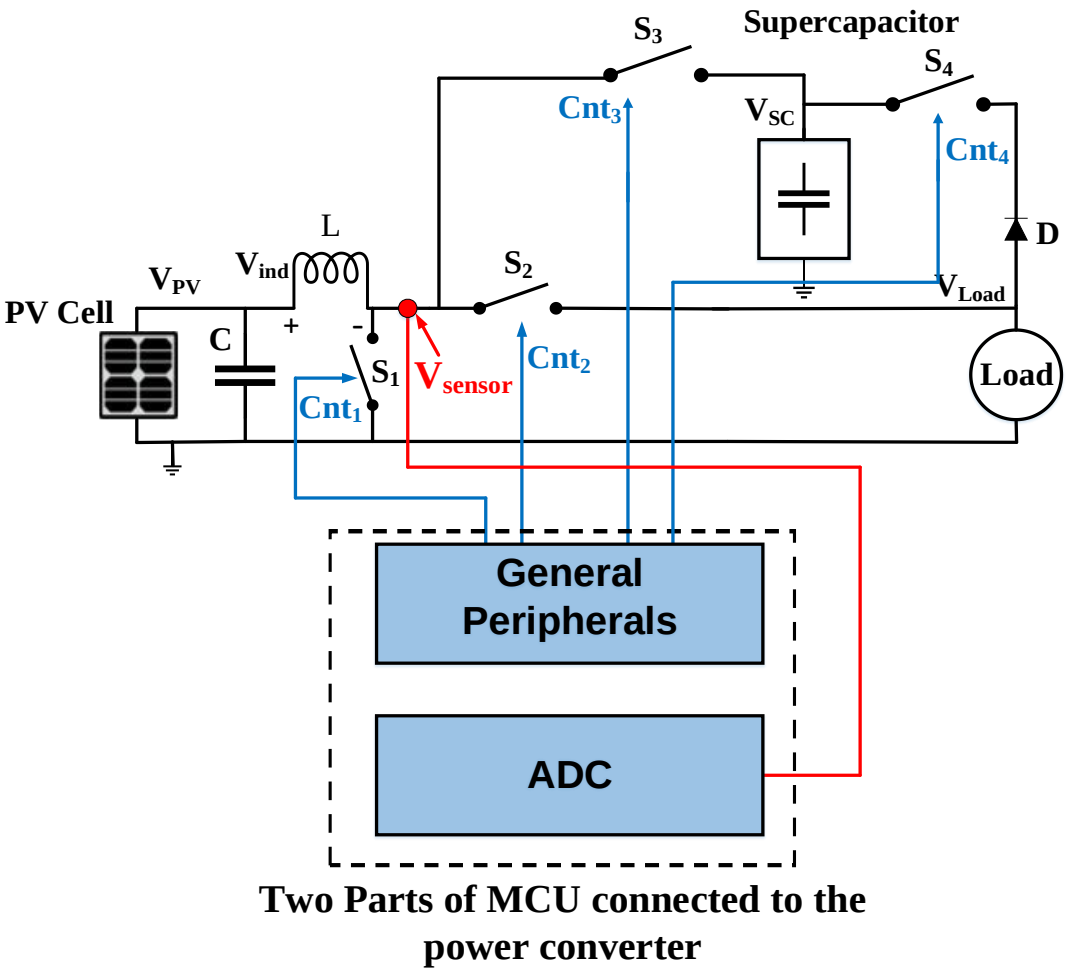

Figure 4.3 Block diagram of the proposed energy harvesting solution

This is a considerable advantage over the current hardware-based solutions as the firmware can be written to ensure maximum energy extraction under various scenarios.

4.3.1 Open Circuit Voltage MPPT Using MCU

Maximum Power Point Tracking (MPPT) is an algorithm to extract maximum power from a PV module under varying environmental factors. There are many algorithms to extract maximum energy from a PV module. They are different in cost, hardware designs, number

of parameters, speed, and complexity [53]. MPPT circuits are usually embedded in DC-DC converters like boost, buck, boost-buck converter.

To extract maximum energy from the PV cell in Figure 4.3, an open circuit voltage methodology [5] is implemented in which the ADC in the MCU is used to read the PV cell open circuit voltage, V_{OC}. The novelty of the proposed method is that it does not need any additional switch to get V_{OC} in contrast with the conventional open circuit MPPT. When all four switches are in the off state, the MCU commands the ADC to sense the voltage from V_{sensor} location of the boost converter circuit which is connected to the ADC pin of the MCU. This analog voltage is equal to V_{OC}. In the next step, when S_1 turns on, the ADC again sense V_{sensor}, which is considered as the voltage across the PV cell which varies with the indoor light intensity, V_{PV}. To minimize the power consumption in the MPPT mode, MCU sets a very low duty cycle of 1% which is just enough to sample V_{PV}. The flowchart in Figure 4.4 indicates the steps taken to control the process of energy harvesting for maximum energy efficiency.

The sampled open circuit voltage is converted to digital data and used to track the maximum power point. The MCU adjusts the frequency and the ON time for switches to ensure that :

$$V_{PV} = 0.76 * V_{OC} \tag{4-1}$$

It is empirically proven that the maximum energy is extracted from the PV cell if equation (4-1) holds. The performance of MPPT algorithm indicates that the V_{OC} is linearly proportional to V_{MPP} [29]. The calculated V_{PV} is saved as a reference voltage, V_{Ref}, for the converter to control the duty cycle of PWM signals and select the operation mode of the

boost converter. When V_{Ref} falls below the V_{OC}, the duty cycle is increased to deliver more energy to the load, and when V_{Ref} exceeds the V_{OC}, the duty-cycle is decreased.

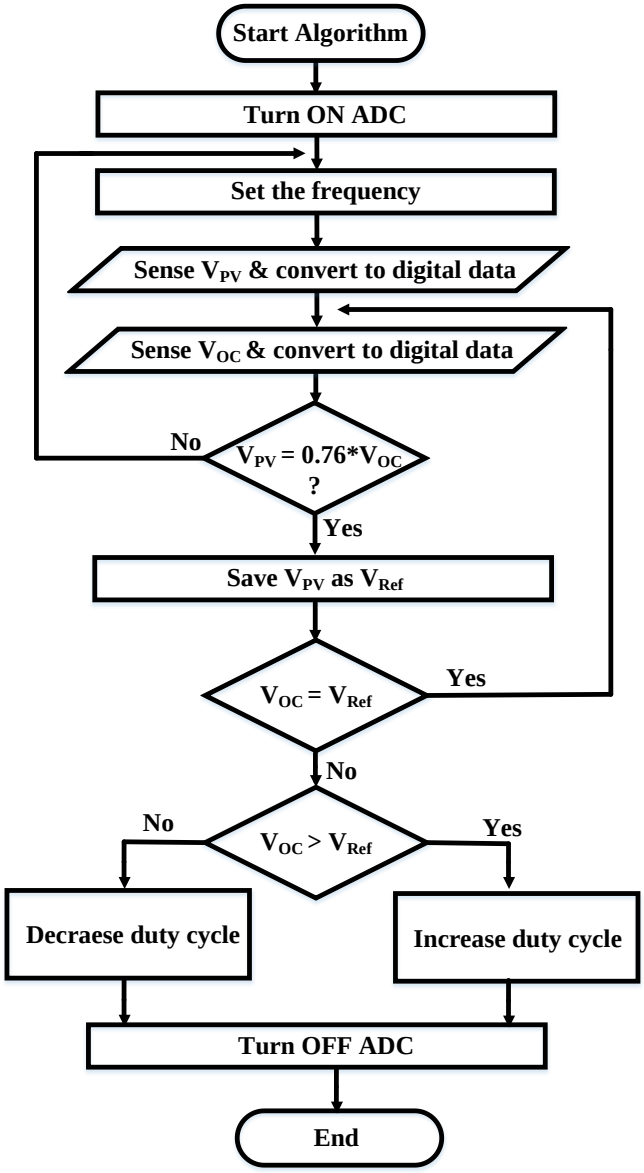

Figure 4.4 Flowchart of the proposed open circuit voltage MPPT method

4.3.2 Boost Converter Analysis

A boost converter can work either in a discrete current mode or in a continues current mode. If the boost converter works in the Continues Current Mode (CCM), the current flows through the inductor continuously [55].

In this mode, if the duration of one complete cycle is represented by T_{Total}, the duration of ON time, T_{ON}, for S_1 is represented by:

$$T_{ON} = T_{Total} * D \tag{4-2}$$

Where D is a fraction of duty-cycle which is set by the MCU. Likewise, the duration of time when S_1 is off, T_{OFF}, is given by:

$$T_{OFF} = T_{Total} * (1 - D) \tag{4-3}$$

Assuming continues current mode we can write:

$$V_{PV} * T_{ON} = (V_{Load} - V_{PV}) * T_{OFF} \tag{4-4}$$

Substitute (4-2) (4-3) to (4-4):

$$V_{PV} * T_{Total} * D = (V_{Load} - V_{PV})(1 - D) * T_{Total} \tag{4-5}$$

It is simplified to:

$$V_{Load} = \frac{V_{PV}}{(1-D)} \tag{4-6}$$

Equation (4-6) shows that the load voltage can be determined by the input voltage, V_{PV}, and the duration of T_{ON} with respect to the total period, D. T_{ON} has to be properly calculated

to reduce the output ripple, lower the switching loss and limit the maximum current in the inductor.

When the output load current falls below a certain level, the converter works in Discontinues Current Mode (DCM) and the current in the inductor becomes zero for a certain period of time and then rises until the next switching cycle.

The duration of ON state of the switch in DCM is:

$$T_{ON} = T_{Total} * D \tag{4-7}$$

And the duration of the OFF state is:

$$T_{OFF} = T_{Total} * D2 \tag{4-8}$$

During the T_{ON}, the inductor current increases as:

$$\Delta_{IL} = \frac{V_L}{L} * D * T_{Total} \tag{4-9}$$

Where Δ_{IL} is the magnitude of ripple current. The T_{ON} and T_{OFF} states in DCM is shown in Figure 4.6.

4.3.3 Peak Inductor Current in Boost Converter Circuit

A large T_{ON} may damage the inductor. Figure 4.6 represents the inductor current in the DCM mode when S_1 and S_2 are on in the recycle mode. From t_0 to t_1 when Cnt_1 is enabled and S_1 is on, in the rising edge of the clock cycle, the inductor current increases linearly and it may exceed the maximum nominal current of the inductor. From t_1 to t_2 when s_1 is off and S_2 is on, in the rising edge of the clock, the inductor current starts to decrease as the current is delivered to the load. Figure 4.8 shows the switching cycles variation and the

changes in the inductor current in the backup mode. When S_3 is on between t_0 to t_1 the inductor current increases in the reverse direction to charge C_1. In practice, T_{ON} and the duty-cycle are adjusted by the MCU based on the open circuit voltage across the PV cell and the load voltage to limit the current passing through the inductor. The duty-cycle is considered to be dynamic to allow the energy harvesting system to operate efficiently under different light intensity conditions. After each sampling event, the duty cycle is calculated by the MCU to determine T_{ON}. Moreover, T_{ON} should not exceed the maximum value of $T_{ON\text{-}max}$ to ensure that the inductor current remains lower than the nominal peak current [56], I_{Peak} , which is defined by:

$$I_{Peak} = \int_0^{TON-max} \frac{V_{PV}-V_{Load}-I_{ind}(t)*R_S}{L} dt \quad (4\text{-}10)$$

Where I_{ind} is the instantaneous inductor current, R_S is the inductor resistance plus the resistance of S_1 when it is on and L is the inductance.

4.4 The Proposed Boost Converter Circuit

The energy harvesting system in this method consists of only a boost converter circuit and an MCU to execute the algorithm through firmware for maximum energy extraction, and generate PWM with appropriate duty-cycle to enable switches. So, the converter can distribute balanced energy between the load and the supercapacitor. Four-switch single-inductor dual-input boost converter is implemented in this design to efficiently deliver constant power to the load. The reuse of the MCU has eliminated the needs for the control and the mode determination circuits. In the proposed method, there are two modes of operation, (a) when the available PV cell energy is lower than the energy required by the load (Recycle mode) and (b) when the available PV cell energy is higher than what is

needed by the load (Backup mode). The proposed energy harvesting system either works in the recycle mode or in the backup mode. The mode detection algorithm and PWM sequences are coded in the firmware and executed by the MCU.

4.4.1 Recycle Mode Operation

The MCU is utilized to determine which mode of operation must be selected for the proposed boost converter. The capability of switching to different converter's operation modes allows the converter to work efficiently and deliver an adequate energy to the load under different circumstances. In the recycle mode, shown in Figure 4.5, the energy extracted from the PV cell is enough to turn on the load. In this mode, the converter works with two switching phases. The MCU uses its embedded 12-bit ADC and 48MHz frequency to sample V_{PV} and V_{LOAD} in every energy checker process. In the recycle mode, the energy generated by the PV cell exceeds the energy consumed by the load. In this mode, initially, it is assumed that S_4 is always on and S_3 is always off.

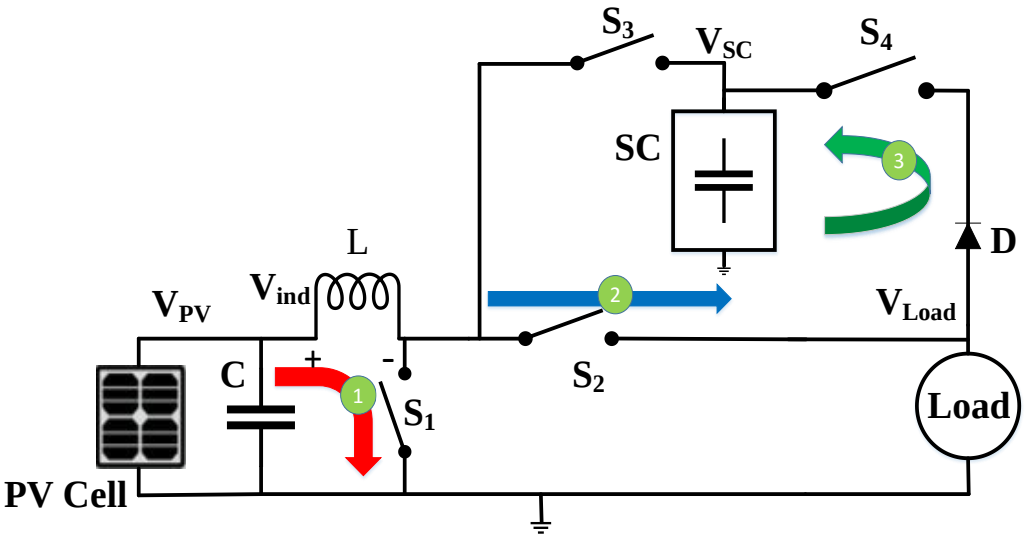

Figure 4.5 Three phases of energy transfer in the recycle-mode

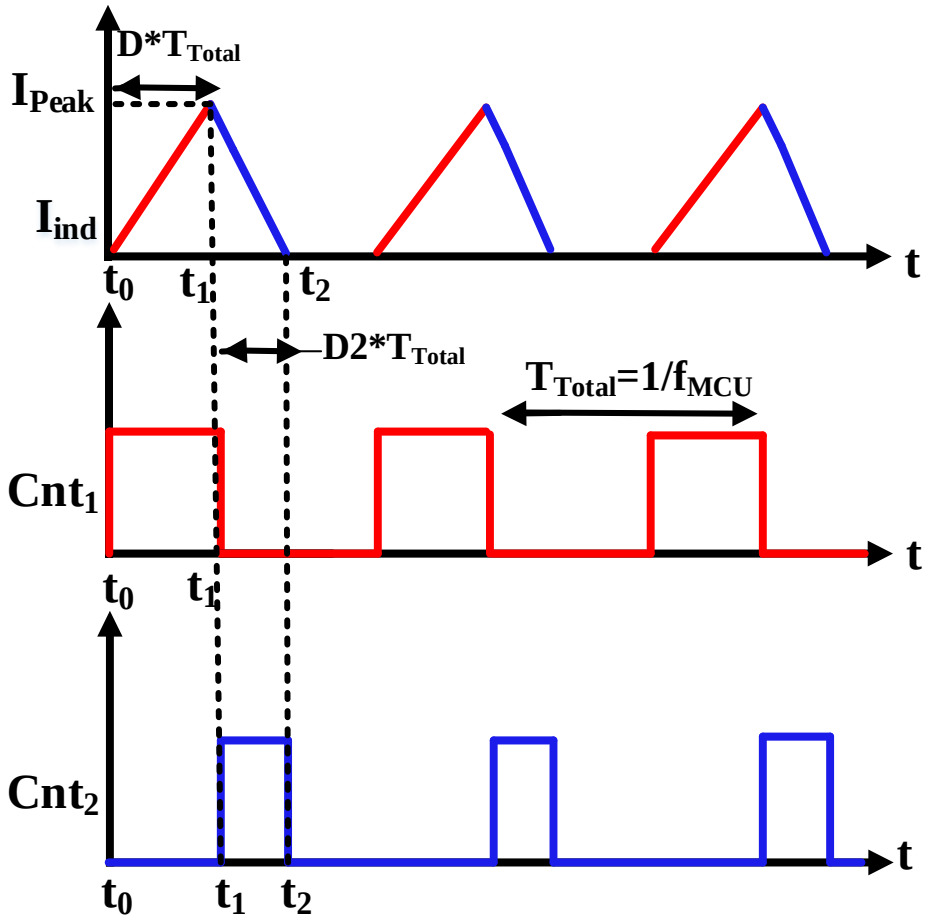

Figure 4.6 Switch control signals variations and the inductor current changes in recycle mode

The MCU turns on S_1 for the duration of T_{ON} to convert the electrical energy stored in C_1 to magnetic energy in the inductor. At the second phase, S_2 is turned on to transfer the energy to the load and pass the surplus energy to the supercapacitor. The paths of energy transmission for the three phases of operation in the recycle mode are shown in Figure 4.5. The PWM control signals, generated specifically for this mode, are shown in Figure 4.6.

4.4.2 Backup Mode Operation

In the backup mode, the V_{PV} is not enough to supply the load, so the supercapacitor assists the PV cell to supply the load. Figure 4.7 shows that in this mode, first S_4 is turned off to separate the load from the supercapacitor. Then S_3 turns on and C_1 is charged through the inductor. Then S_3 is turned off and S_1 is turned on to transfer the energy to the inductor. Finally, in the third phase, S_1 turns off and S_2 turns on to transfer the energy from the inductor to the load. In the backup mode, the energy stored inside C_1, E_{C1}, is initially supplied through both PV cell which is given by $E_{C1}=\frac{1}{2}C_1V_{PV}^2$. This is not enough to power on the load and the required energy of the load has to be supplied by the supercapacitor to turn on the load. When S_3 is turned on, the energy in C_1 elevates to $E_{C1}=\frac{1}{2}C_1V_{SE}^2$ .Where V_{SC} is the voltage across the supercapacitor. Thus, the surplus energy supplied by the storage element is given by:

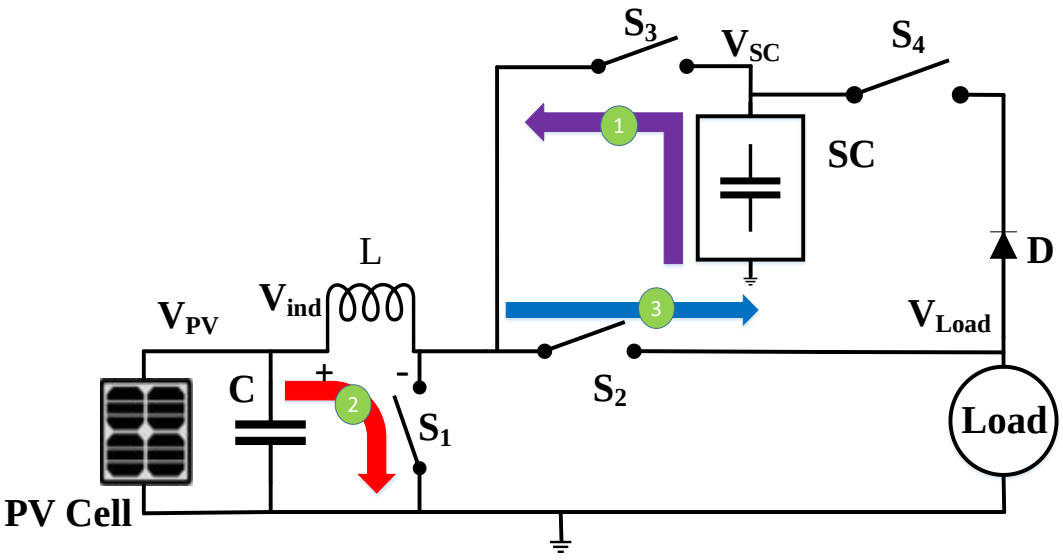

Figure 4.7 Paths of energy transfer in the backup mode

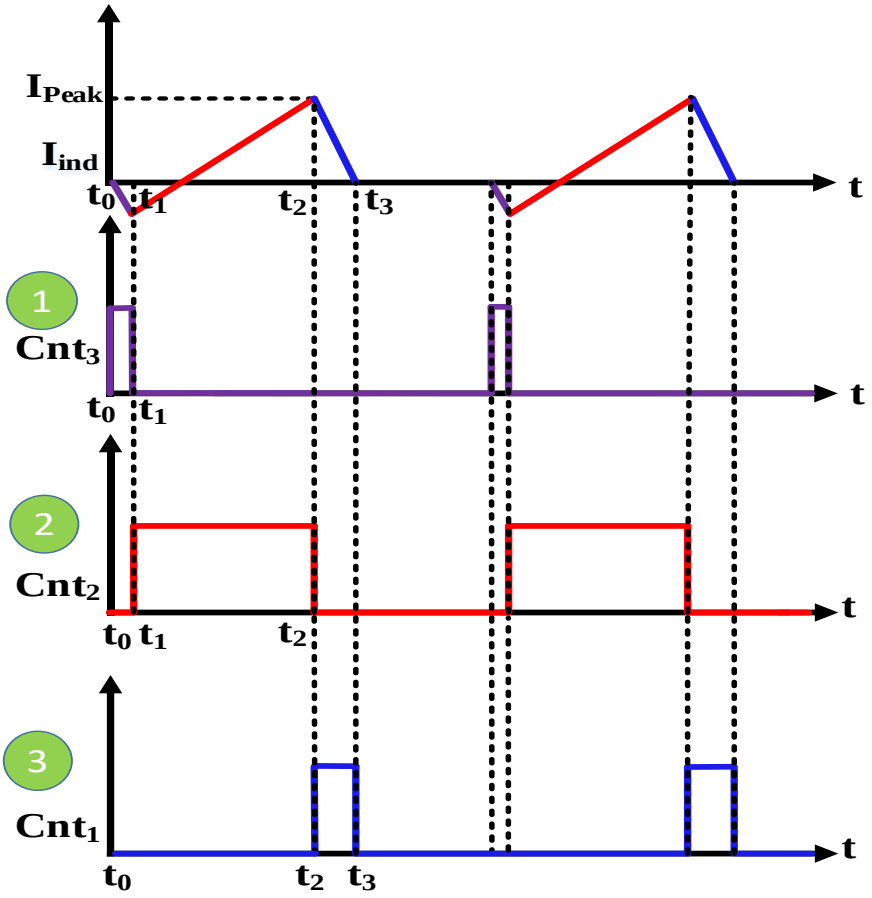

Figure 4.8 Switch control signals variations and inductor current changes in backup-mode

$$E_{C1} = \frac{1}{2} C_1 (V_{SC}^2 - V_{PV}^2) \quad (4\text{-}11)$$

The use of MCU in the proposed solution adds the capacity to the energy harvester to readily adapt to a situation where the light intensity drops significantly. In this case, the frequency of sensing the PV cell voltage decreases and the sleep time for the sensor is extended to ensure operation over a longer time period. Figure 4.8 indicates the three PWM control signals in backup mode and the changes in the inductor current. When S_3 turns on

for the duration of t_0 to t_1, a charge packet transfer to C1 and then rises the inductor current in the opposite direction. In the next state, when S_2 is turned on from t_1 to t_2, the inductor current becomes zero and then increases in the forward path to store the energy in the inductor. In the third state, the stored energy in the inductor is used to supply the load with its nominal voltage level for the duration of t_2 to t_3.

4.5 Storage Element

As the light intensity can change considerably, the energy delivered by the PV cell as a primary source may not be adequate to power on the load. Therefore, a secondary energy supplier is considered. Moreover, sometimes the extracted energy by the PV cell exceeds the load requirement, so the energy harvesting circuit needs a storage element to store the surplus energy. A supercapacitor or a battery can be used as a storage element, but it is much better to use a supercapacitor because it has the advantage of a long life and it can charge even with non-constant voltage in contrast to rechargeable batteries [57].

Nevertheless, a supercapacitor suffers from self-leakage current which restricts the usage of this element in conventional energy harvesting systems for IoT applications [58]. A supercapacitor with 1F capacity and a nominal voltage of 3.6V is used in parallel with the load to store the energy and supply the load when it is needed. In the proposed circuit in Figure 4.3, a diode, D, is placed between the supercapacitor and the load to prevent discharge in the recycle mode when S_4 is on. In the proposed energy harvesting system for IoT sensors, the supply voltage of the employed IoT sensor is 3V [51].

The energy stored in the supercapacitor, E_{SC} is calculated by:

$$E_{SC}=\frac{1}{2}CV_{SC}^2 \tag{4-12}$$

Where C is the capacitance of the supercapacitor in F, and V_{SC} is the voltage across the supercapacitor.

4.6 The PWM Control Signal Method of the Boost Converter

The PWM signal is utilized to control the proposed boost converter circuit which can be generated by a timer interrupt in the MCU. There are four general-purpose timer module in the MCU, and each one can support four PWM and runs on 48MHz [51]. In the proposed method in CC2650, GPTimer is utilized to generate PWM which is employed as an enable signal of switches in the energy harvesting system to control the process of energy distribution. The duty cycle of PWM signals can be changed anytime to change the energy harvesting mode.

4.7 Mode Detection of Boost Converter Using ADC and MCU

In order to determine the mode of operation, the MCU compares the power extracted from the PV, P_{PV}, with the power delivered to the load power, P_{Load}. The process of extracting maximum energy through conventional energy harvesters requires an advanced control module and an accurate PWM circuit.

The mode transmission algorithm of the converter is shown in Figure 4.9. The sensor is connected to the energy harvesting PCB board through the Develop Pack connector of the sensor tag. The steps taken to mode detection of the boost converter is described as follows. The algorithm is set to run every 5 minutes if the sensor is not in the communication mode, the MCU is programmed to enter the energy checker mode. All idle blocks in the MCU are turned off to lower the power consumption for energy harvesting system. When the MCU enters the energy harvesting mode, it first turns on the ADC only to sense the voltage and then the MCU performs OCV MPPT and samples the open circuit voltage level across the

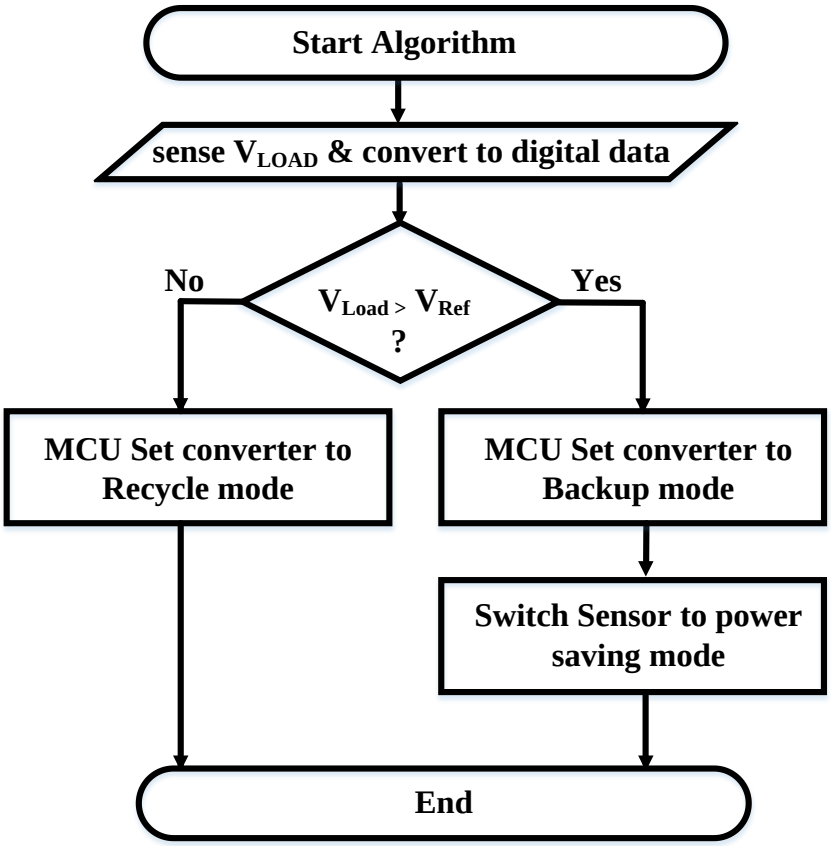

Figure 4.9 Mode transmission algorithm

PV cell, V_{oc}, The ADC converts the value of the sensed analog voltage to a 12-bit digital number and sends it to the CPU for processing. The CUP performs an algorithm to check the MPPT, and then the value of V_{PV} is stored as V_{Ref}. The MCU calculates the duty-cycle and uses V_{Ref} for comparison in the mode transmission algorithm. If the CPU detects that V_{PV} exceeds the value of V_{Ref} by more than 5% then it decreases the value of duty cycle, D. Then CPU interrupts the Timer to generate PWM with T_{Total} of 200ns and adjust T_{ON} according to the value of calculated D to perform the recycle-mode operation. The flow chart of mode transmission of the proposed energy harvesting system is shown in Figure 4.9. The transmission to different modes depends on the light intensity and the load power consumption.

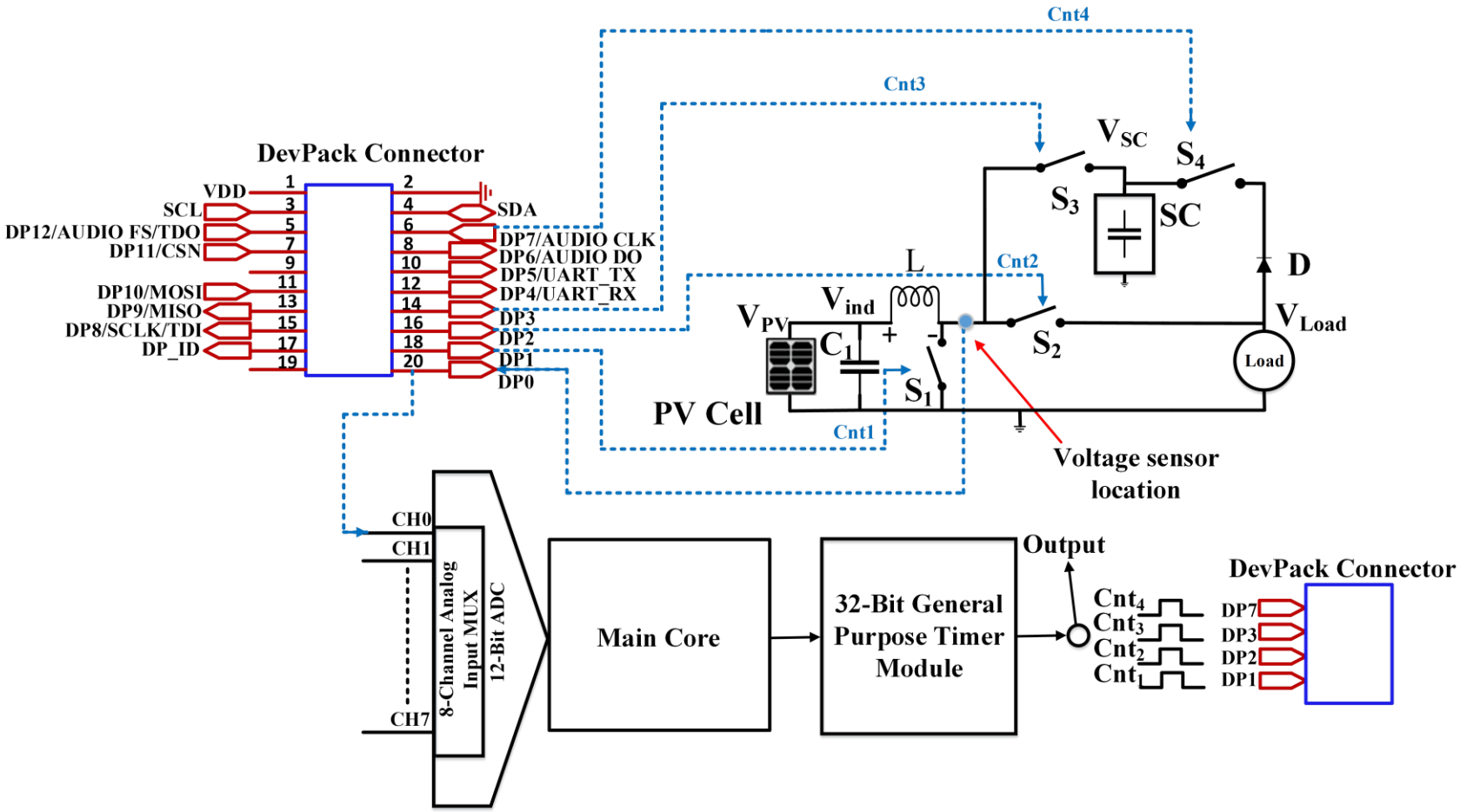

Figure 4.10 The proposed energy harvesting circuit and connection map to TI sensor tag

When V_{Load} increases, the power consumption decreases and when V_{Load} exceeds V_{Ref}, the MCU changes the converter mode from the backup mode to the recycle mode and it decreases the duty-cycle. In this case, the PV module supplies the load and transfers the surplus energy to the supercapacitor. If the MCU detects that V_{Load} is lower than $V_{Ref,}$ it changes the converter operation mode from recycling mode to the backup mode. On the other hand, when changes occur in the V_{PV}, the MCU detects the variation and changes the converter mode.

4.8 Energy harvesting System Connections To the MCU

As shown in Figure 4.10 the enable pin of S_1 is connected to DP1, S_2 to DP2, S_3 to DP3, and S_4 to DP7. DP1 to DP4 are the input/output pins of the DevelopPack connector. This connector is utilized in our work to connect the energy harvesting board to the sensor. In the recycle mode, two generated PWM signals, Cnt_1 and Cnt_2, are sent to the converter through DP1 and DP2, respectively.

In the backup-mode, the CPU set T_{OFF} to turn S_4 off by Cnt_4 which is connected to DP7 and holds the switch off until it detects that the converter should change the mode to the recycle-mode. There is also an extreme case of operation where the MCU detects that V_{PV} has fallen more than 5% and the V_{SC} is also fallen more than 10%, and neither the ambient energy nor the stored energy is adequate to continue the sensor operation. In this case, the MCU reduces the sensor's sampling frequency and increase its overall sleep time to allow the operation over a longer period of time. Therefore, the proposed boost converter circuit works with two states in the recycle mode and works with 4 states in the backup mode.

4.9 Simulation Results

The proposed boost converter circuit was implemented to power on a commercially available smart sensor of CC2650 known as Sensortag. The harvester is designed to work with a minimum light intensity of 200Lux which is available in most indoor environments. The input capacitor C_1 was chosen to be 10μF and the inductor value was selected to be 10μH and C_2 was chosen to be 5μF. It is calculated that the MCU in the sensor tag consumes 1.45mA in the active mode and 1μA in the sleep mode. The proposed boost converter circuit is designed and simulated in Cadence design environment. Simulations were performed for different indoor light intensity. Figure 4.11 illustrates the simulation results of the proposed boost converter for a case where the harvester operates in the recycle mode with approximately 200 lux light intensity. The control gate signals for S_1 and S_2 are indicated as Ctn_1 and Cnt_2 respectively. The control voltage for S_1, Ctn_1, is turned on 40% in each cycle to boost the input voltage V_{PV}. It can be observed that the load voltage is boosted to 3V and the load is supplied with 5.5mA current. The inductor current, I_{ind}, shows that the converter works in the continuous mode.

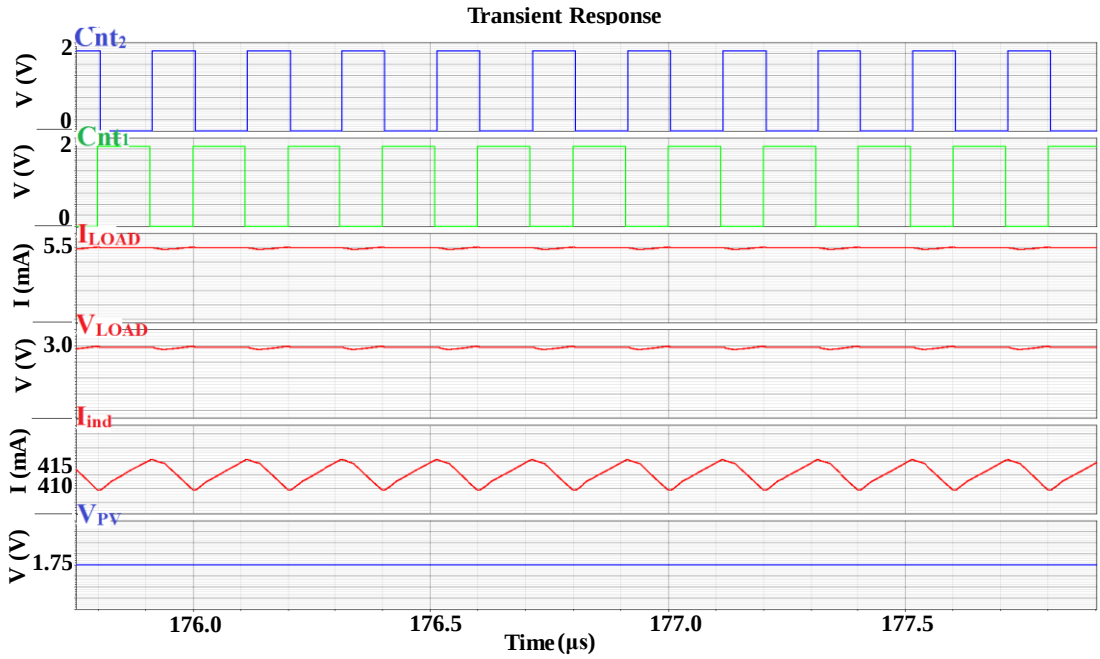

Figure 4.11 Recycle mode simulation with duty-cycle of 40% when sensor is in active mode

Figure 4.12 shows the simulation results in the backup mode where the PV voltage is 350mV and the light intensity drops to approximately, 50 Lux. The voltage across the load is about 510mV which falls lower than the nominal load voltage. The power consumed by the MCU to control the harvesting process is low compared to the reported methods where discrete components are used to implement the control circuitry. The ADC is turned on for a short period of time to sample the voltage levels in different modes. It consumes 22.5µW and for the implemented algorithm to track MPP voltage every 20s, the power consumption is about 1.125nW. The power consumption of the control circuits for the implemented algorithm which utilizes a timer in the MCU to generate control signal every 20s is about 250nW. Table 4.2 compares the results of this work with previously reported works. The proposed solution has a wide dynamic range as compared to the reported solution and can operate when the input voltage is very low as 350mV.

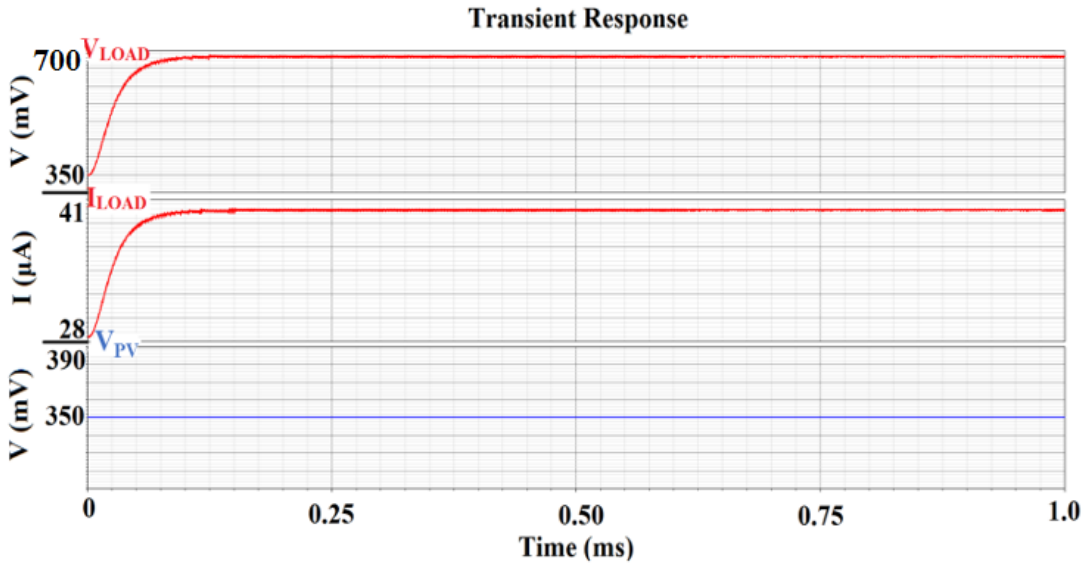

Figure 4.12 Backup mode simulation with duty-cycle of 50% when the sensor is in active mode

Table 4.2 Comparision with conventional energy harvesting systems

	[29]	**[59]**	**[56]**	**[28]**	**This work**
Inductor	47 µH	1mH	220µH	10 µH	10μH
V_{PV}	2~4V	0.5~2V	0.5V	2.6V	350mV~ 3.5V
No. of Switches	5	2	3	7	5
Power consumption	_	1.95 µW	_	400 nW	250 nW

Moreover, it consumes much lower power and while using a limited number of external components.

4.10 Energy Harvesting System Fabrication

The proposed boost converter has been designed and implemented on as a PCB. The PCB is designed by Altium PCB Design software which is shown in Figure 4.13. The energy harvesting board has dimensions of 53.47mm ×38.35mm×1.6mm. The PV module, the supercapacitor, and C1 are mounted on the top layer of the PCB and all other components are soldered on the bottom side of the PCB board.

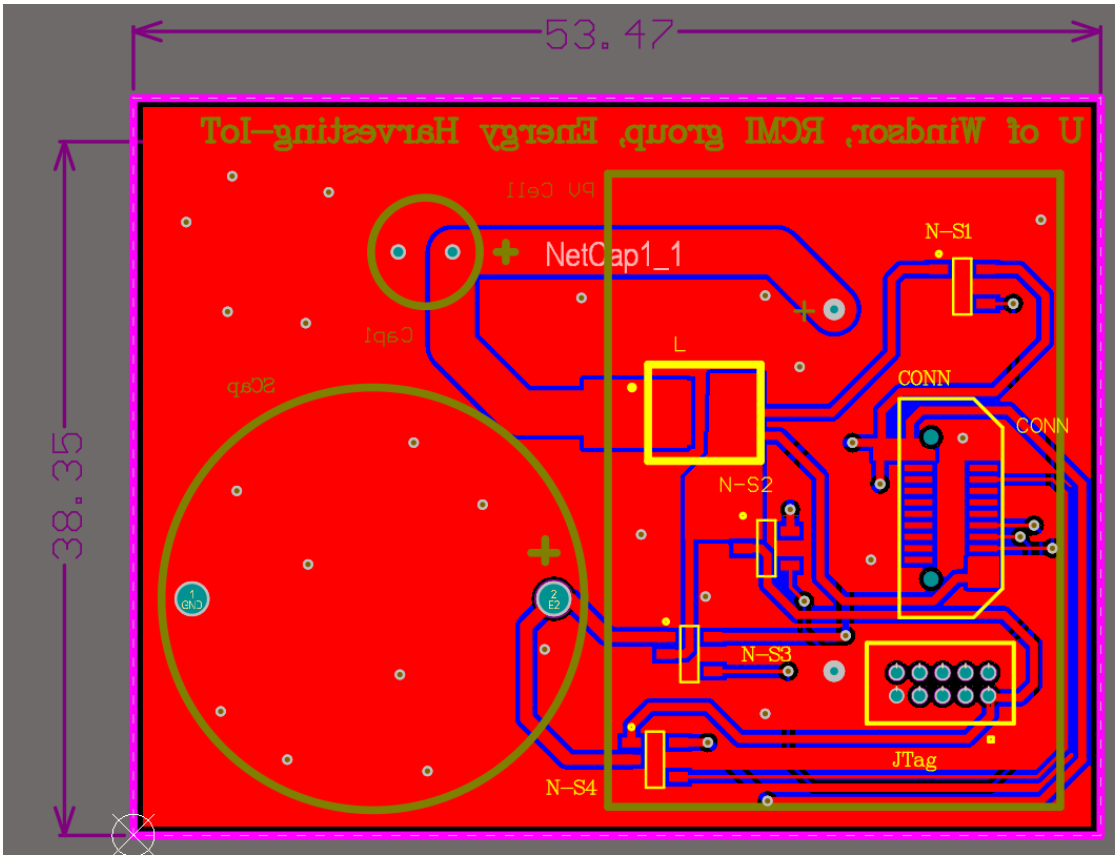

Figure 4.13 The layout of fabricated energy harvesting system in Altium software

Table 4.3. Component utilized for the proposed energy harvesting system circuit

Component name	**Value**
PV cell	16.8mW
Inductor	10µH
Buffer capacitor (C1)	6.8µF
Supercapacitor	1F

The Amorphous Silicon solar cell with dimensions of 25mm×20mm which can generate maximum power of 16.8mW is utilized [60]. The circuit components are listed in Table 4.3. The PCB is connected to the sensor tag by Conn Hermaphroditic and Jtag connectors. Figure 4.14 (A) shows the top side of the fabricated energy harvesting board, and Figure 4.14 (B) shows the cross view of the board which is mounted on the TI sensor tag via two connectors.

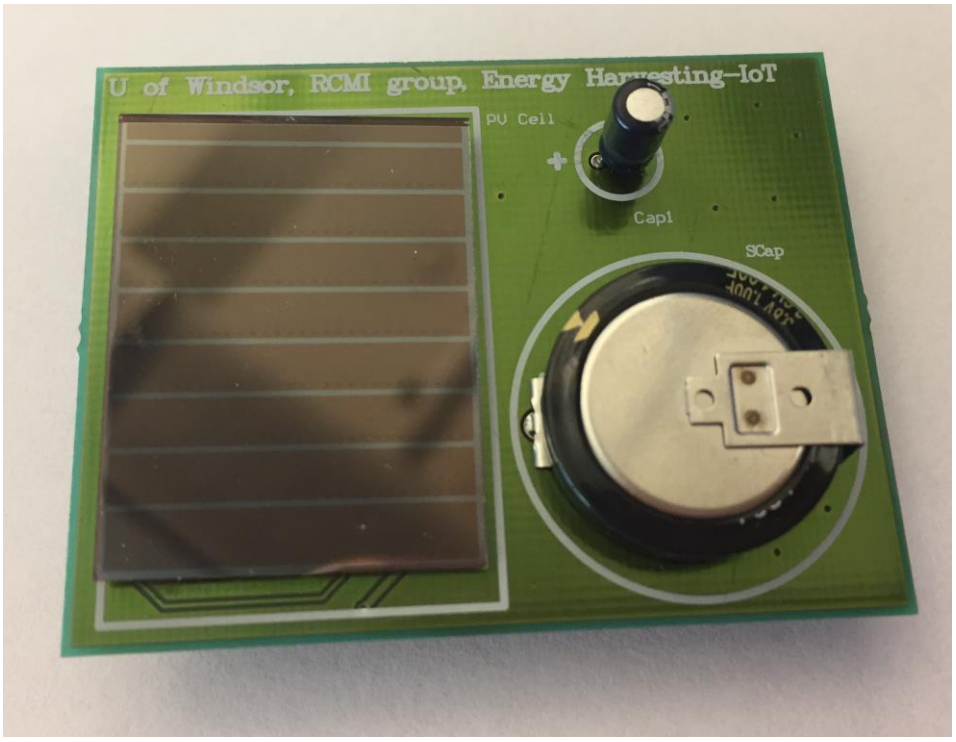

(A)

(B)

Figure 4.14 (A) Top view of 53.47mm ×38.35mm×1.6mm fabricated energy harvesting board. (B) Cross view of energy harvesting board mounted on TI sensor tag

4.11 Conclusion

A new method of energy harvesting for IoT smart sensors is developed in which the available resources inside the sensor are reused for energy harvesting system. The operation of the smart sensor is controlled by a low power microcontroller. The MCU in the smart sensor is reused to implement an advanced energy harvesting algorithm with a minimum number of external components. The energy harvester can operate in the recycle mode or in the backup mode depending on the available energy supplied by a photovoltaic cell. The energy harvester utilizes a boost converter circuit with four switches and a single inductor. The proposed boost converter is implemented on PCB board. The results show that the proposed solution can efficiently provide the energy needed for a smart sensor in an indoor environment with light intensity as low as 200 Lux.

CHAPTER V

CONCLUSION AND FUTURE WORK

6.1 Conclusions

Billions of wireless IoT sensors are predicted to be installed by 2020. The energy harvesting which is proposed and implemented in this work overcomes the problems associated with the use of batteries. The light energy in both outdoor and indoor environments can be harvested to power on low-power sensors.

In this work, first, a boost DC-DC converter utilizing MEMS switches was presented and used as the building block of an energy harvester. The use of MEMS switches in the converter increases the overall energy harvesting efficiency. A low-actuation voltage MEMS switch is designed, and then three MEMS switches are utilized to implement a boost converter. Simulation results indicate that the implemented MEMS-based boost converter increases the efficiency by about 17% compared to a boost converter using transistor-based switches.

The designed boost DC-DC converter is used to power a commercially available IoT sensor. The hardware resources of the IoT sensor were reused to implement the energy harvester. Using the MCU resources reduces the area overhead, power consumption, and simplifies the control process.

6.2 Future Work

In this thesis, an energy harvesting system is designed and fabricated which is controlled by the MCU on the sensor. There is room to further improve the efficiency through an advanced software-based algorithm to simultaneously maximize the energy harvesting and minimize the energy consumption by the control circuitry. Moreover, an energy harvesting solution using all the available ambient resources including light, vibration and electromagnetic waves can be developed to increase the overall energy harvesting efficiency.

REFERENCES

[1] Egham, "Gartner Says 8.4 Billion Connected." *Hype Cycle Research Methodology | Gartner Inc.*, Gartner, Inc, 2017. [Online]. Available: http:// www.gartner.com/newsroom/id/3598917. [Accessed: 10- May- 2018].

[2] J.M, Morgan, "A Simple Explanation Of 'The Internet Of Things", 2014. [Online]. Available: https://www.forbes.com/sites/jacobmorgan/2014/05/13/simple-explanation-internet-things-that-anyone-can-understand/#2380d95d1d09. [Accessed: 16- March-2018].

[3] M.B, Burgess, "What Is the Internet of Things? WIRED Explains." *WIRED*, WIRED UK, 16 Feb, 2018. [Online]. Available: http:// www.wired.co.uk/article/internet-of-things-what-is-explained-iot. [Accessed: 16- March-2018].

[4] M.G, Gipson, "Sensors - The Lifeblood of the Internet of Things." *SemiElectronics*, 6 Oct, 2017. [Online]. Available: https://semielectronics.com/sensors-lifeblood-internet-things. [Accessed: 16- March- 2018].

[5] IoT Made Easy." *PC & Notebooks IC Solutions| Overview| TI.com*, 2015. [Online]. Available: http:// www.ti.com/ww/en/wireless_connectivity/sensortag/. [Accessed : 16- March- 2018].

[6] "Wireless Sensor Network." , 24 Aug, 2016. [Online]. Available: http://www.ni.com/white-paper/7142/en/. [Accessed :16- March-2018].

[7] R. J. M. Vullers, R. V. Schaijk, H. J. Visser, J. Penders, and C. V. Hoof, "Energy harvesting for autonomous wireless sensor networks," *IEEE Solid-State Circuits Mag.*, vol. 2, no. 2, pp. 29–38, Spring, 2010.

[8] Carvalho, Carlos, and Nuno Paulino. "On the Feasibility of Indoor Light Energy Harvesting for Wireless Sensor Networks." *Procedia Technology*, vol. 17, pp. 343–350, 2014.

[9] M.M. Merry, "Environmental Problems That Batteries Cause.", 13 March, 2013. [Online]. Available: https://sciencing.com/environmental-problems-batteries-cause-7584347.html. [Accessed: 18- March- 2018].

[10] A.T, Theron-Ord, "ZigBee partners with EnOcean to extend energy harvesting benefits", *Meteringcom*, 15 Mar, 2016. [Online]. Available: https:// www.metering.com/regional-news/europe-uk/zigbee-partners-enocean-extend-energy-harvesting-benefits/. [Accessed: 20-March-2018].

[11] L. Xin, and S.H. Yang, "Thermal energy harvesting for WSNs." *2010 IEEE International Conference on Systems, Man and Cybernetics* , PP. 3045-3052, 2010.

[12] S. Vignati, "Solutions for Indoor Light Energy Harvesting," *M.S. thesis, Commun. Systems Dept. Kungliga Tekniska Högskolan*, Stockholm, Sweden, 2012.

[13] F. Goldschmidtboeing, and P. Woias, "Characterization of Different Beam Shapes for Piezoelectric Energy Harvesting." *Journal of Micromechanics and Microengineering*, vol. 18, no. 10, p. 104013, 2008.

[14] H. O, Ostaffe, “RF Energy Harvesting Enables Wireless Sensor Networks.” *Sensors Magazine*, 13 Oct, 2009. [Online]. Available: https://www.sensorsmag.com/components/rf-energy-harvesting-enables-wireless-sensor-networks. [Accessed: 22- March- 2018].

[15] M. P. Aparicio, A. Bakkali, J. Pelegri-Sebastia, T. Spgorb, V. Llario, and A. Bou, “Radio frequency energy harvesting - sources and techniques”. *Renewable Energy - Utilisation and System Integration*, (pp.155- 170), 2016.

[16] Manuel, Ferreira Carvalho Carlos, and Paulino Nuno Filipe Silva Veríssimo. *CMOS Indoor Light Energy Harvesting System for Wireless Sensing Applications*. Springer International Publishing, 2016.

[17] “DC-to-DC Converter.”, *Wikipedia*, Wikimedia Foundation, 10 Apr, 2018. [Online]. Available: http:// en.wikipedia.org/wiki/DC-to-DC_converter. [Accessed: 22-March-2018].

[18] A. Nasiri, S. A. Zabalawi, and G. Mandic, "Indoor power harvesting using photovoltaic cells for low-power applications, " *IEEE Transactions on Industrial Electronics*, vol. 56, issue 11, PP. 4502-4509, 2009.

[19] J. Ahmad, "Fractional open circuit voltage based maximum power point tracker for photovoltaic arrays, " *2nd International Conference on Software Technology and Engineering (ICTE)*, vol. 1, pp. V1-247- V1-250, 2010.

[20] W.-C. Liu, Y.-H. Wang, and T.-H. Kuo, “An adaptive load-line tuning IC for photovoltaic module integrated mobile device with 470 μs transient time, over 99% steady-

state accuracy and 94% power conversion efficiency," in *IEEE ISSCC Dig. Tech. Papers*, pp. 70–71, Feb. 2013,

[21] Y. Nakase *et al.*, "0.5 V start-up 87% efficiency 0.75 mm2 on-chip feedforward single-inductor dual-output (SIDO) boost DC-DC converter for battery and solar cell operation sensor network micro-computer integration," *IEEE J. Solid-State Circuits*, vol. 48, no. 8, pp. 1933–1942, Aug. 2013.

[22] A. Shrivastava, Y. K. Ramadass, S. Khanna, S. Bartling, and B. H. Calhoun, "l," in *IEEE Symp. VLSI Circuits Dig. Tech. Papers*, pp. 1–2, Jun. 2014.

[23] S. Bandyopadhyay, and A. P. Chandrakasan, "Platform architecture for solar, thermal, and vibration energy combining with MPPT and single inductor," *IEEE J. Solid-State Circuits*, vol. 47, no. 9, pp. 2199–2215, Sep. 2012.

[24] S. Bandyopadhyay, and A. P. Chandrakasan, "Platform architecture for solar, thermal and vibration energy combining with MPPT and single inductor," in *IEEE Symp. VLSI Circuits Dig. Tech. Papers*, pp. 238–239, Jun. 2011.

[25] S. Kim and G. A. Rincón-Mora, "Dual-source single-inductor 0.18 μm CMOS charger-supply with nested hysteretic and adaptive on-time PWM control," in *IEEE ISSCC Dig. Tech. Papers*, pp. 400–401, Feb. 2014.

[26] M. Chen and G. A. Rincon-Mora, "Single inductor, multiple input multiple output (SIMIMO) power mixer-charger-supply system," in *Proc. Int. Symp. Low Power Electron. Design*, pp. 310–315, 2007.

[27] N.M. Sze, F. Su, Y. H. Lam, W.H. Ki, and C. Y. Tsui, “Integrated single inductor dual-input dual-output boost converter for energy harvesting applications,” in *Proc. IEEE Int. Symp. Circuits Syst.*, pp. 2218–2221, May. 2008.

[28] G. Yu, K. W. R. Chew, Z. C. Sun, H. Tang, and L. Siek, “A 400 nW single-inductor dual-input–tri-output DC–DC buck–boost converter with maximum power point tracking for indoor photovoltaic energy harvesting,”*IEEE J. Solid-State Circuits*, vol. 50, no. 11, pp. 2758–2772, Nov. 2015.

[29] H. Shao, X. Li, C.-Y. Tsui, and W.-H. Ki, “A novel single-inductor dual input dual-output DC–DC converter with PWM control for solar energy harvesting system,” *IEEE Trans. Very Large Scale Integr. (VLSI) Syst.*, vol. 22, no. 8, pp. 1693–1704, Aug. 2014.

[30] H.-J. Chen, Y.-H. Wang, P.-C. Huang, and T.-H. Kuo, “An energy recycling three-switch single-inductor dual-input buck/boost DC-DC converter with 93% peak conversion efficiency and 0.5mm2 active area for light energy harvesting,” in *Solid- State Circuits Conference - (ISSCC), 2015 IEEE International*, pp. 1–3, 2015.

[31] X. Meng, X. Li, C. Y. Tsui, W.H. Ki , "An indoor solar energy harvesting system using dual mode SIDO converter with fully digital time-based MPPT," 2016 IEEE International Symposium on Circuits and Systems (ISCAS), pp. 2354-2357, 2016.

[32] S. Kim and G. A. Rincón-Mora, “Dual-source single-inductor 0.18 μm CMOS charger-supply with nested hysteretic and adaptive on-time PWM control,” in *IEEE ISSCC Dig. Tech. Papers*, pp. 400–401, Feb. 2014.

[33] B.S. Deepaksubramanyan, and A. Nunez, “Analysis of Subthreshold Leakage Reduction in CMOS Digital Circuits.” *2007 50th Midwest Symposium on Circuits and Systems*, 2007.

[34] V. A. Raj, “MEMS-based multi-Band Energy Harvesting for Wireless Sensor Network applications.” 2016 International Conference on Energy Efficient Technologies for Sustainability (ICEETS), 2016.

[35] M. Daneshmand, “Multi-port RF MEMS switches and switch matrices,” Ph.D. dissertation, Univ. Waterloo, Waterloo, ON, Canada, Jan. 2006.

[36] K. Khodadady, and B. A. Ganji, “Design and Modeling of a Novel RF MEMS Series Switch with Low Actuation Voltage.” Microsystem Technologies, vol. 22, no. 12, pp. 2921–2929, 2015.

[37] H. Jaafar, F. L. Nan, and N. A. M. Yunus, “Design and Simulation of High Performance RF MEMS Series Switch.” *2011 IEEE Regional Symposium on Micro and Nano Electronics*, 2011.

[38] A. S. Khan, and T. Shanmuganantham. “Simulation and Analysis of RF MEMS Cantilever Switch for Low Actuation Voltage.” *2017 IEEE International Conference on Circuits and Systems (ICCS)*, 2017.

[39] G. M. Rebeiz, and J. B. Muldavin, “RF MEMS Switches and Switch Circuits.” *IEEE Microwave Magazine*, vol. 2, no. 4, pp. 59–71, 2001.

[40] D. Peroulis, S. P. Pacheco, and L. P. B. Katehi, “RF MEMS Switches With Enhanced Power-Handling Capabilities.” *IEEE Transactions on Microwave Theory and Techniques*, vol. 52, no. 1, pp. 59–68, 2004.

[41] D. Molinero, S. Cunningham, and A. Morris, “New Power Handling Characterization for RF MEMS Capacitive Switches.” *2017 47th European Microwave Conference (EuMC)*, 2017.

[42] C. Chu, X. Liao, and H. Yan, “Ka-Band RF MEMS Capacitive Switch with Low Loss, High Isolation, Long-Term Reliability and High Power Handling Based on GaAs MMIC Technology.” *IET Microwaves, Antennas & Propagation*, vol. 11, no. 6, pp. 942–948, Dec. 2017.

[43] C. D. Patel, and G. M. Rebeiz, “An RF-MEMS Switch for High-Power Applications.” *2012 IEEE/MTT-S International Microwave Symposium Digest*, 2012.

[44] S. H. Song, S. Kang, K. Park, S. Shin, H. Kim, “Applications of MEMS-MOSFET Hybrid Switches to Power Management Circuits for Energy Harvesting Systems.” Journal of Power Electronics, vol. 12, no. 6, pp. 954–959, 2012.

[45] R. Raman, T. Shanmuganantham, and D. Sindhanaiselvi, “Analysis of RF MEMS Series Switch with Serpentine Spring Shaped Cantilever Beam for Wireless Applications.” Materials Today: Proceedings, vol. 5, no. 1, pp. 1890–1896, 2018.

[46] A. Attaran, and R. Rashidzadeh, “Ultra Low Actuation Voltage RF MEMS Switch.” Micro and Nano Systems Letters, vol. 3, no. 1, Nov. 2015.

[47] J. Tonfat, G. Flach, and R. Reis, “Leakage Current Analysis in Static CMOS Logic Gates for a Transistor Network Design Approach.” 2016 26th International Workshop on Power and Timing Modeling, Optimization and Simulation (PATMOS), pp. 107–113, 2016.

[48] G. M. Rebeiz, “ *RF MEMS: Theory, Design, and Technology”*. Wiley, 2003.

[49] A. A. Elbaset, H. Ali, M. A. E. Sattar, and M. Khaled, “Implementation of a Modified Perturb and Observe Maximum Power Point Tracking Algorithm for Photovoltaic System Using an Embedded Microcontroller.” *IET Renewable Power Generation*, vol. 10, no. 4, Jan. 2016, pp. 551–560, 2015.

[50] P. Das, “Maximum Power Tracking Based Open Circuit Voltage Method for PV System.” *Energy Procedia*, vol. 90, pp. 2–13, 2016.

[51] Texas Instruments. CC2650 SimpleLink Multistandard Wireless MCU, accessed on Sep. 12, 2016. [Online]. Available:http://www.ti.com/lit/ds/symlink/cc2650.pdf

[52] J. Lindh, C. Lee, and M. Hernes, “Measuring Bluetooth Low Energy Power Consumption”, Jan 2017. [Online]. Available: http:// http://www.ti.com/lit/an/swra478c/swra478c.pdf. [Accessed: 14- Feb- 2018].

[53] B. R. Sanjeeva Reddy, P. Badari Narayana, P. Jambholkar, and K. Srinivasa , “MPPT Algorithm Implementation for Solar Photovoltaic Module Using Microcontroller.” *2011 Annual IEEE India Conference*, 2011.

[54] J. Ahmad, "Fractional open circuit voltage based maximum power point tracker for photovoltaic arrays, " 2nd International Conference on Software Technology and Engineering (ICTE), vol. 1, pp. V1-247- V1-250, 2010.

[55] E. Rogers, " Understanding Boost Power Stages in Switchmode Power Supplies", March 1999. [Online]. Available: https://www.ti.com.cn/cn/lit/an/slva061/slva061.pdf. [Accessed: 2- Jun- 2018].

[56] H.-H. Wu, C.-L. Wei, Y.-C. Hsu, and R. B. Darling, "Adaptive Peak-Inductor-Current-Controlled PFM Boost Converter With a Near-Threshold Startup Voltage and High Efficiency, " IEEE Transactions on Power Electronics, vol. 30, no. 4, pp. 1956–1965, 2015.

[57] "Coupling a Supercapacitor with a Small Energy Harvesting Source." *EETimes*, Jan 2012. [Online]. Available: https://www.eetimes.com/document.asp?doc_id=1279362. [Accessed: 2- June- 2018].

[58] H. G. Lee and N. Chang, "Powering the IoT: Storage-less and converter less energy harvesting," in Proc. 20th Asia South Pacific Design Autom.Conf, pp. 124–129, 2015.

[59] Y. Qiu, C. V. Liempd, B. O. H. Veld, P. G. Blanken, and C. V. Hoof, "5μW-to-10mW input power range inductive boost converter for indoor photovoltaic energy harvesting with integrated maximum power point tracking algorithm, " Solid-State Circuits Conference-(ISSCC), 2011 IEEE International, pp.118-120, 2011.

[60] "World's Largest Selection of Electronic Components Available for Immediate Shipment!®." [Online]. Available:

https://www.digikey.com/products/en?keywords=%09869-1009-ND. [Accessed: 16- Feb-2018].

[61] X. Yue, M. Kauer, M. Bellanger, O. Beard, M. Brownlow, D. Gibson, C. Clark, C. MacGregor, S. Song, "Development of an Indoor Photovoltaic Energy Harvesting Module for Autonomous Sensors in Building Air Quality Applications." *IEEE Internet of Things Journal*, vol. 4, no. 6, pp. 2092–2103, 2017.

VITA AUCTORIS

NAME: Maryam Eshaghi

PLACE OF BIRTH: Isfahan, Iran

YEAR OF BIRTH: 1990

Education:

Master of Applied Science (Electrical Engineering)	June 2018
University of Windsor	Windsor, ON
Bachelor of Science (Computer Engineering)	January 2013
Islamic Azad University	Isfahan, Iran